THESIS FOR THE DEGREE OF LICENTIATE OF ENGINEERING

Driving stability of passenger vehicles under crosswinds

ADAM BRANDT

Department of Mechanics and Maritime Sciences

CHALMERS UNIVERSITY OF TECHNOLOGY

Göteborg, Sweden 2021

Driving stability of passenger vehicles under crosswinds
ADAM BRANDT

Thesis for the degree of Licentiate of Engineering 2021:03
ISSN 1652-8565
Department of Mechanics and Maritime Sciences
Chalmers University of Technology
SE-412 96 Göteborg
Sweden
Telephone: +46 (0)31-772 1000

Chalmers Digitaltryck
Göteborg, Sweden 2021

Driving stability of passenger vehicles under crosswinds
ADAM BRANDT
Department of Mechanics and Maritime Sciences
Chalmers University of Technology

Abstract

Passenger cars are a vital part of modern society, giving people the freedom of flexible travel. As technology advances, customers increase their demands for future products. The automotive industry must, therefore, adapt to society's requirements of energy-efficient travel, where developing low drag vehicles is key. However, if not designed with care, streamlined bodies of low drag might impair driving stability. In addition, raised customer demands of perceived control and stability elevate the research needs on driving stability in crosswinds.

Vehicles travelling on open roads are always exposed to the changing crosswind conditions. Most road vehicles have the aerodynamic centre of pressure located at the front half of the vehicle, making them sensitive to these crosswinds. Strong winds and sensitive vehicle designs may degrade the perceived level of driving stability by drivers and passengers. In extreme winds, this can even cause accidents. Furthermore, the aerodynamic loads increase with flow velocity, deteriorating the driving stability performance at higher speeds.

The assessment of driving stability in the development of a new vehicle is often done at the test tracks during late design phases when prototype vehicles are available. However, the current demands of faster development times require robust virtual methods for assessing the stability performance in early design phases. The goal of this thesis is, therefore, to find virtual simulation tools for assessing straight-line driving stability, and to gain more insights on the interdisciplinary physics between aerodynamics and vehicle dynamics.

By conducting experimental on-track measurement, it was confirmed that crosswinds deteriorate the driving stability and that the vehicle motions of lateral acceleration and yaw velocity correlate with the drivers' subjective assessment. These motions were combined into a proxy measure for stability, later used for objective assessment in the numerical simulations. The numerical study employed a coupled simulation methodology between aerodynamics and vehicle dynamics. It was shown that a 1-way coupling was sufficient for passenger vehicles in normal wind conditions. Furthermore, the aerodynamic loads, including the yaw moment overshoots during transient gust events, could accurately be predicted by a quasi-steady model accounting for the phase delay between axles when driving into crosswinds. An extensive parametric study highlighted the aerodynamic yaw moment coefficient and the longitudinal centre of gravity position as the two most influential vehicle parameters. In addition, the suspension characteristics revealed potential in improving the driving stability performance under crosswinds.

Keywords: aerodynamics, vehicle dynamics, driving stability, crosswind, high speed

Acknowledgements

First of all, I would like to thank my supervisors Prof. Simone Sebben and Prof. Bengt Jacobson for all the guidance and support throughout the years improving the quality of my work. I would also like to thank Prof. Ingemar Johansson for his dedication and initialisation of this research project. The project includes colleagues from CEVT (China Euro Vehicle Technology), namely Jan Hellberg, Dr. Robert Moestam and Jörgen Sjöström, who have given valuable support and showed great willingness to collaborate interdisciplinarily. A special thanks to my manager Erik Preihs for always believing in me and supporting me when needed the most.

Much of the experimental work would not have been possible without the kind people at VCC (Volvo Car Corporation) and Hällered Proving Ground, lending me experimental equipment. I would also like to thank Sören Andersson for his help and for our daily commutes to the proving ground during the experimental phase of my project. Next, I would like to thank Samuel Gabriel and Mattias Olander, working at CEVT CAE Aerodynamics, for their discussions and advice regarding CFD and the stock market.

Furthermore, I want to show appreciation to my former and present colleagues and friends at VEAS for creating an excellent work environment incorporating both valued academic discussions and entertaining activities.

Last but not least, I want to thank my friends and especially my family for supporting and encouraging me from the very start. To Fanny, thank you for everything. Especially that you put up with spending all awake time with me in our small one-room apartment during these strange times.

Adam Brandt
Göteborg, January 2021

Nomenclature

Abbreviations

CAE	Computer-Aided Engineering
CEVT	China Euro Vehicle Technology
CFD	Computational Fluid Dynamics
CoG	Centre of Gravity
CP	Centre of Pressure
DES	Detached Eddy Simulation
DoF	Degree of Freedom
GPS	Global Positioning System
IMU	Inertial Measurement Unit
LES	Large Eddy Simulations
MBD	Multi-Body Dynamic
NSP	Neutral Steering Point
QS	Quasi-Steady (aerodynamic model)
QSD	Quasi-Steady with axle Delay (aerodynamic model)
RANS	Reynolds-Averaged Navier-Stokes
RTK	Real-Time Kinematic
SBES	Stress-Blended Eddy Simulation
SUV	Sports Utility Vehicle
tCFD	Transient CFD (aerodynamic simulation technique)
TI	Turbulence Intensity
VCC	Volvo Car Corporation

Symbols

α	Lateral slip angle	[rad]
β	Vehicle body slip angle	[deg]
Δ	Change	
δ_{SW}	Steering wheel angle	[deg]
δ_f	Front axle steer angle	[rad]
δ_r	Rear axle steer angle	[rad]
λ	Crosswinds length scale	[m]
ω_x	Roll velocity	[deg/s]
ω_y	Pitch velocity	[deg/s]

ω_z	Yaw velocity	[deg/s]
ψ	Relative flow angle	[deg]
ρ	Density of air	[kg/m^3]
St	Stroughal number	[-]
$\vec{\omega}$	Vehicle body angular velocity vector	[deg/s]
$\vec{a}$	Vehicle body acceleration vector	[m/s^2]
$\vec{F}_{aero}$	Aerodynamic loads	[N & Nm]
$\vec{V}$	Relative flow vector	[m/s]
$\vec{w}$	Wind vector	[m/s]
$\vec{z}_t$	Road vertical wheel input vector	[m]
A	Vehicle frontal area	[m^2]
a_x	Longitudinal acceleration	[m/s^2]
a_y	Lateral acceleration	[m/s^2]
a_z	Vertical acceleration	[m/s^2]
C_f	Front axle lateral tire cornering stiffness	[N/rad]
C_{lf}	Aerodynamic coefficient of front lift force	[-]
C_{lr}	Aerodynamic coefficient of rear lift force	[-]
C_L	Aerodynamic coefficient of lift force	[-]
C_r	Rear axle lateral tire cornering stiffness	[N/rad]
C_S	Aerodynamic coefficient of side force	[-]
C_{ym}	Aerodynamic yaw moment coefficient	[-]
C_y	Lateral tire cornering stiffness	[N/rad]
d_{fRC}	Front axle roll damping	[Nm/(deg/s)]
d_{rRC}	Rear axle roll damping	[Nm/(deg/s)]
f	Frequency	[Hz]
F_{flz}	Front left normal tire force	[N]
F_{frz}	Front right normal tire force	[N]
F_{fyw}	Front axle lateral tire force	[N]
F_{lf}	Aerodynamic front axle lift force	[N]
F_{lr}	Aerodynamic rear axle lift force	[N]
F_L	Aerodynamic lift force	[N]
F_{rlz}	Rear left normal tire force	[N]
F_{rrz}	Rear right normal tire force	[N]
F_{ryw}	Rear axle lateral tire force	[N]
F_{sf}	Aerodynamic front axle side force	[N]

F_{sr}	Aerodynamic rear axle side force	[N]
F_S	Aerodynamic side force	[N]
F_{yt}	Lateral tire forces	[N]
h	Centre of gravity height	[m]
h_{fRC}	Front axle roll centre height	[m]
h_{rRC}	Rear axle roll centre height	[m]
J_s	Vehicle sprung mass moment of roll inertia	[kgm^2]
J_z	Vehicle mass moment of yaw inertia	[kgm^2]
K	Reduced frequency	[-]
$K_1 = \frac{1}{2}\rho A$	Constant for simplification	[kg/m]
K_2	Aerodynamic side force coefficient gradient	[1/deg]
k_{fRC}	Front axle roll stiffness	[N/deg]
k_{rRC}	Rear axle roll stiffness	[N/deg]
L	Wheel base	[m]
l_{CP}	Distance between mid-axle reference and CP	[m]
l_{NSP}	Distance between mid-axle reference and NSP	[m]
l_f	Distance between CoG and front axle	[m]
l_r	Distance between CoG and rear axle	[m]
l_s	Distance between CoG and NSP	[m]
L_v	Vehicle length	[m]
m	Vehicle mass	[kg]
M_x	Aerodynamic roll moment (ref. at ground mid-axles)	[Nm]
M_y	Aerodynamic pitch moment (ref. at ground mid-axles)	[Nm]
M_z	Aerodynamic yaw moment (ref. at ground mid-axles)	[Nm]
t	Time	[s]
t_0	Gust start time	[s]
t_{gust}	Gust duration	[s]
T_{SW}	Steering wheel torque	[Nm]
t_b	Gust build-up time	[s]
t_d	Gust drop time	[s]
t_p	Gust pause time	[s]
U	Flow mean velocity	[m/s]
$u^{'}$	Flow velocity fluctuations	[m/s]
V_{mag}	Relative flow magnitude	[m/s]
v_x	Vehicle longitudinal velocity	[m/s]

w_x	Longitudinal wind component	[m/s]
w_y	Crosswind component	[m/s]
w_y^{end}	Gust end amplitude	[m/s]
w_y^{max}	Gust maximum amplitude	[m/s]
w_y^{min}	Gust minimum amplitude	[m/s]
w_y^{start}	Gust start amplitude	[m/s]
x	Longitudinal distance	[m]
Y	Combined proxy measure for driving stability	
y^+	Non-dimensional wall distance	[-]

Definitions

High speed	$>100\,\text{km/h}$

Thesis

This thesis consists of an extended summary and the following appended papers:

Paper A Brandt, A., Sebben, S., Jacobson, B., Preihs, E., and Johansson, I. "Quantitative High Speed Stability Assessment of a Sports Utility Vehicle and Classification of Wind Gust Profiles". *SAE Technical Paper Series*. 2020. DOI: 10.4271/2020-01-0677

Paper B Brandt, A., Jacobson, B., and Sebben, S. "High Speed Driving Stability of Road Vehicles under Crosswinds: An aerodynamic and vehicle dynamic parametric sensitivity analysis". *Submitted to Vehicle System Dynamics* (2020)

Division of work

A All instrumentation setup, data acquisition and analysis for Paper A was done by Brandt. The high speed driving at the test track was performed by Brandt and two experienced test drivers. The first manuscript was written by Brandt then discussed, reviewed and revised by all authors.

B The aerodynamic simulations and quasi-steady modelling were performed by Brandt. The vehicle dynamic reference model (MBD high-fidelity) was created by the Vehicle Dynamics CAE team at CEVT. Brandt constructed the low- and mid-fidelity models, performed the coupled simulations and constructed the parametric sensitivity study. The first manuscript was written by Brandt then discussed, reviewed and revised by all authors.

Contents

Abstract i

Acknowledgements iii

Nomenclature v

Thesis ix

Contents xi

I Extended summary 1

1 Introduction 3
- 1.1 Research objectives . . . 4
- 1.2 Limitations . . . 4
- 1.3 Outline . . . 5

2 Background 7
- 2.1 On-road wind conditions . . . 8
- 2.2 Driver behaviour and subjective assessment . . . 10
  - 2.2.1 Driver behaviour . . . 10
  - 2.2.2 Subjective assessment . . . 10
- 2.3 Road vehicle dynamics . . . 11
  - 2.3.1 Vehicle dynamic straight-line handling . . . 11
  - 2.3.2 Crosswind aerodynamics . . . 13
  - 2.3.3 Numerical modelling and simulations . . . 17
- 2.4 Vehicle development process . . . 18

3 Experimental study on driving stability 21
- 3.1 Experimental setup . . . 21
  - 3.1.1 Instrumentation . . . 21
  - 3.1.2 Test track and test procedure . . . 22
  - 3.1.3 Post-processing . . . 23
- 3.2 Results and discussion . . . 24
  - 3.2.1 Wind load conditions and gust profiles . . . 25
  - 3.2.2 Objective assessment . . . 28

4 Numerical crosswind stability modelling 31
- 4.1 Aerodynamic methodology . . . 32
- 4.2 Vehicle dynamic methodology . . . 34
  - 4.2.1 Classical bicycle model (low fidelity) . . . 35
  - 4.2.2 Enhanced model (mid fidelity) . . . 35
  - 4.2.3 Multi-body dynamic model (high fidelity) . . . 35

4.2.4 Driver modelling 35
4.2.5 Model validation 35
4.3 Coupling methodology 37
4.4 Parametric analysis methodology 38
4.5 Results and discussion 39
4.5.1 Aerodynamic gust modelling 40
4.5.2 2-way coupling analysis 41
4.5.3 Parametric sensitivity analysis 42

5 Concluding remarks **45**
5.1 Future work 46

6 Summary of papers **49**
6.1 Paper A 49
6.2 Paper B 49

References **51**

II Appended papers **55**

Part I

Extended summary

1

Introduction

This thesis is focused on driving stability of passenger vehicles in crosswind conditions, specifically during high speed driving. The work is interdisciplinary, focusing on both the aerodynamic and vehicle dynamic performance related to driving stability.

The passenger car has become a vital part of modern society over the last century. Its flexibility enables decentralised transportation for a large part of the population, seen as a freedom by many. As technology advances, customers acclimatise to the modern solutions and increase their demands for future products. The automotive industry must therefore adapt to the new demands from customers. Today, society requires more energy-efficient travel to reduce the transport sector's negative impact on the environment. For this, developing vehicles with low aerodynamic drag is key. However, streamlined bodies of low drag might impair the driving stability, if not designed with care. This, with the raised customer demands of perceived control and stability in modern cars, have increased the research needs on aerodynamic and vehicle dynamic driving stability.

Vehicles having issues with driving stability are often described as *nervous* by drivers. When driving on the highway, this will force the driver to correct the vehicle to remain in the lane. If this becomes difficult or is required too often, it classifies as a major driving stability issue. Vehicles with excellent driving stability performance will not require any corrections and are perceived as stable even in crosswind conditions. Furthermore, increasing the vehicle speed tends to further deteriorate the stability performance. *High speed stability* is discussed in this work, where high speed is defined as $>100\,\mathrm{km/h}$. High speed stability is a subset of *driving stability*. These definitions cover stability regardless of crosswinds or not. Hence, *crosswind stability* is another subset of driving stability. It is presumed that either crosswinds or high speeds are required to impair the stability performance. As stated above, this work focus on driving stability under crosswinds at high speeds.

In the development of a new passenger vehicle, the evaluation of driving stability at high speeds is often done subjectively using prototype vehicles. Unfortunately, prototype vehicles are only available at a late stage in the development process and changes at these stages are costly and difficult to implement. Issues with driving stability are therefore difficult to deal with and it can be challenging to find balanced compromises for improving driving stability, since this can affect other vehicle attributes. A way to resolve this would be to move the assessment from the on-track testing to the virtual world, using numerical tools. This has received increased interest during the last decades, with the improvements in computational performance. A virtual

assessment of driving stability can be used in early design phases, enabling improvements when the cost of change is lower and removing most issues before the prototype vehicles are built. However, it is expected that the final evaluation still needs to be done at the test tracks.

1.1 Research objectives

The objectives of this research project are to increase the knowledge on driving stability performance of passenger vehicles and to understand how virtual simulation methods can be used to develop more stable vehicles. Three research questions have been formulated for the project:

1. How do vehicle dynamics, vehicle aerodynamics and their coupled effect influence vehicle driving stability at high speeds?

2. What quantities can objectively rate the vehicle driving stability and how can they be considered in the development process?

3. Which virtual methods can be used to develop and evaluate the driving stability performance of a passenger vehicle?

The first question aims at understanding the interdisciplinary physics, while the second focuses on setting better engineering requirement to prevent issues with driving stability. The last question elaborates on how to move the assessment of driving stability from the road to the virtual environment by using simulation tools.

1.2 Limitations

- The test track time and measurement equipment have been limiting resources during the experimental testing. The numerical resources are also limited in terms of computational power, model accuracy and simulation techniques.

- Only one vehicle has been used as a research object in this thesis. Figure 1.1 show a rendered image of the compact sports utility vehicle (SUV) from the numerical study. The corresponding vehicle model was used in the experimental study. The vehicle was front wheel driven, with a total length of 4.51 m, a height of 1.60 m, a width of 1.86 m and a wheel base of 2.73 m. The curb weight of the vehicle was 1856 kg, with 56 % of the static load on the front axle. The vehicle was fitted with 235/50 R19 tires. The suspension system consisted of a MacPherson front suspension and a 4-link trailing arm rear suspension. Coil springs and passive dampers control the suspension system. The steering system has a steering rack with an electrical power-assisted servo function.

- The visuals, acoustics and steering wheel haptics may influence the driver's perception of driving stability. This work will only consider the body motion of the vehicle as input to the driver's subjective assessments.

1.3 Outline

Chapter 1 provided the context of driving stability and stated the objectives and limitations of the research project. Chapter 2 covers relevant background and theory particularly on realistic on-road wind conditions, crosswinds aerodynamics and straight-line vehicle dynamic handling. Chapters 3 and 4 are focused on an experimental and a numerical study, respectively. These chapters include the specific methodology of each study followed by a discussion on the relevant results for this thesis. Chapter 5 gives some concluding remarks and outlook into possible future work, followed by a summary of the appended papers in Chapter 6.

Figure 1.1: *A rendered image of the vehicle used in the thesis.*

2

Background

Driving stability at high speeds is an interdisciplinary topic. A system overview is presented in Figure 2.1. The causality is indicated as data flow arrows. The ambient on-road environment affects the system via transient wind and the road unevenness. The horizontal wind components (w_x and w_y) together with the vehicle velocity and body slip (v_x and β) form the relative flow conditions subjected to the travelling vehicle (V_{mag} and ψ). In turn, the aerodynamic forces and moments ($\vec{F}_{aero}$) affect the vehicle dynamic response ($\vec{a}$ and $\vec{\omega}$) which influence the driver's reaction (δ_{SW} or T_{SW}) and subjective assessment. This overview has been designed to visualise the system complexity and to guide the reader into the different problem formulations discussed in the thesis.

This chapter describes typical on-road flow conditions and gives a background on driver behaviour and subjective assessment during straight-line handling. The physics of the dynamic system is then introduced, focusing on straight-line handling, crosswind aerodynamics and the numerical coupling between the two disciplines. Finally, to further extend the background for the reader, the topic is presented from the perspective of the vehicle development process in the automotive industry.

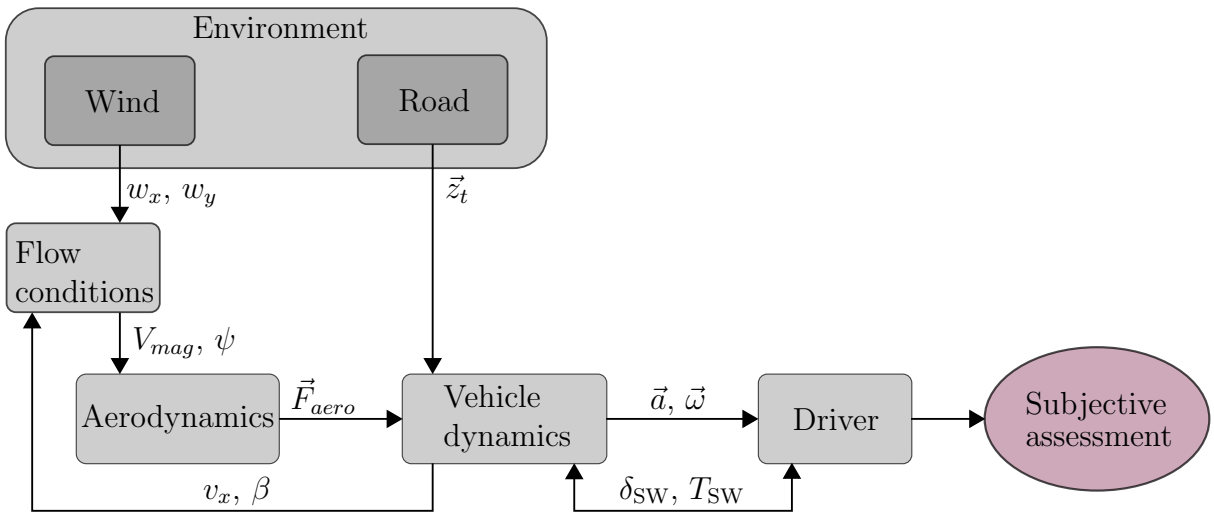

Figure 2.1: *An overview of the system describing vehicle driving stability.*

2.1 On-road wind conditions

Crosswind disturbances are, in principle, always present on open roads. Extreme crosswinds have even shown to increase road accidents [3]. A review by Sims-Williams [4] highlighted that the unsteady flow conditions are caused by the turbulence in the natural wind, flow disturbances by other vehicle and obstacles at the road side. These flow disturbances are formulated below in Equation 2.1 [4].

$$\frac{d\vec{V}}{dt} = \frac{\partial v_x}{\partial t} + \frac{\partial \vec{w}}{\partial t} + v_x \frac{\partial \vec{w}}{\partial x} \tag{2.1}$$

The left-hand side shows the flow transients locally at the vehicle. The right-hand side contains three terms representing the vehicle acceleration, the changing wind conditions (in time) and the flow variation from driving into different wind conditions along the road (Figure 2.2). Sims-Williams argued that the final term is the most influential for a travelling vehicle, meaning that most crosswind gusts originate from driving into different wind conditions ($v_x \frac{\partial \vec{w}}{\partial x}$) rather than local variations in the wind ($\frac{\partial \vec{w}}{\partial t}$) [4].

Another aspect of the on-road flow conditions is the effect of the wind's atmospheric boundary layer. Howell et al. [5] published a paper investigating this effect in 2017. The atmospheric boundary layer creates a sheared crosswind flow, see Figure 2.3. Howell et al. analysed the differences between simulating a uniform crosswind profile, mimicking wind tunnel experiments and traditional CFD setup, to the more realistic sheared crosswind profile. The simulations were designed to produce equal mass flows over the height of the vehicle. The authors found no significant effect on the aerodynamic forces, but added the disclaimer that taller one-box vehicles might experience a larger discrepancy.

The gustiness of the flow is often quantified as turbulence intensity, TI, which is a standard deviation measure using the root-mean-square of the flow fluctuations, $u^{'}$, and the mean velocity, U, as in,

$$TI = \frac{u^{'}}{U}. \tag{2.2}$$

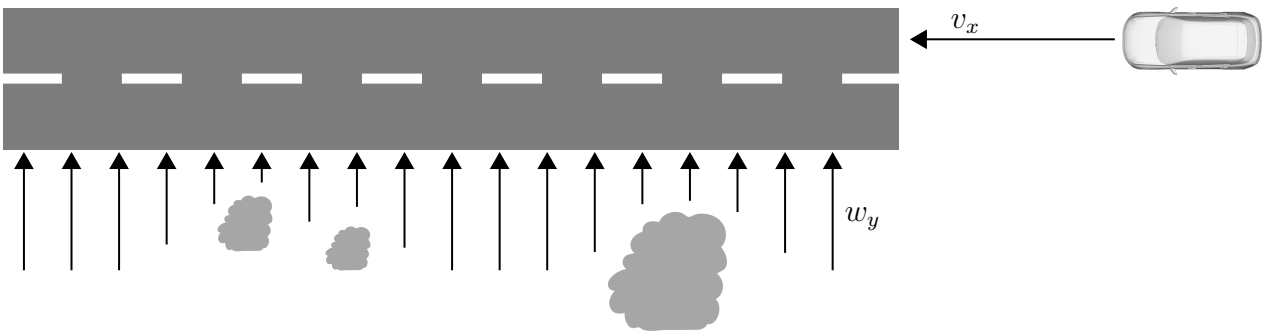

Figure 2.2: *Illustration of the unsteady flow disturbances experienced by a travelling vehicle in spatially steady wind (inspired by [4]).*

The turbulence intensity can differ drastically between the controlled environment of traditional wind tunnels ($TI < 1\,\%$) and the highway traffic seeing up to $TI = 15\,\%$ [6, 7]. Watkins and Cooper [8, 9] presented work on the effects of the atmospheric boundary layer turbulence for road vehicles, based on the theoretical ground work of wind engineering. The experimental data showed good agreement with the von Karman spectrum of homogeneous, isotropic turbulence. The majority of the driving occurred in the turbulence intensity range of 2 % to 10 % [9]. Further, a review showed that the turbulence intensity could alter the optimum design of, for .e.g., the backlight angle of a vehicle, compared to the smooth flow used in most wind tunnels [8]. The literature review by Sims-Williams [4] concluded that crosswind scales of 2-20 vehicle lengths are the most critical for vehicle stability, since there is a significant amount of road spectral energy at these scales and that the vehicle motion response frequencies can not be considered quasi-steady.

Traditional wind tunnels were intentionally designed with low turbulence intensity to increasing the experiments' reproducibility. Similarly, to increase the reproducibility of on-road crosswind experiments, test track facilities with fans to control the external crosswind conditions have been used [10–13]. To standardise experiments at these facilities, the International Standard ISO 12021:2010 [14] was formulated. The guidelines in the ISO 12021:2010 standard include a methodology where a vehicle is driven at 100 km/h into a zone of 20 m/s crosswind, resulting in a flow angle of $\psi = 35.8\,\text{deg}$. The resulting crosswind gust profile has been adopted in several numerical studies of crosswind sensitivity [15–19]. These extreme winds of 20 m/s create high aerodynamic forces and a distinct motion response of the vehicle, useful for measuring differences between vehicles and configurations. However, it has also been shown that these crosswinds are too extreme to represent most real driving scenarios [1, 6, 7, 9, 20–23], and are more likely investigations of extreme crosswind sensitivity, rather than driving stability performance at high speeds. For example, when conducting on-road measurements of crosswind gusts in Germany, Theissen and Wojciak [20, 21] found that the typical magnitude of the crosswind resulted in flow angles between 2 to 10 deg. Similar results were found by Lawson et al. [24].

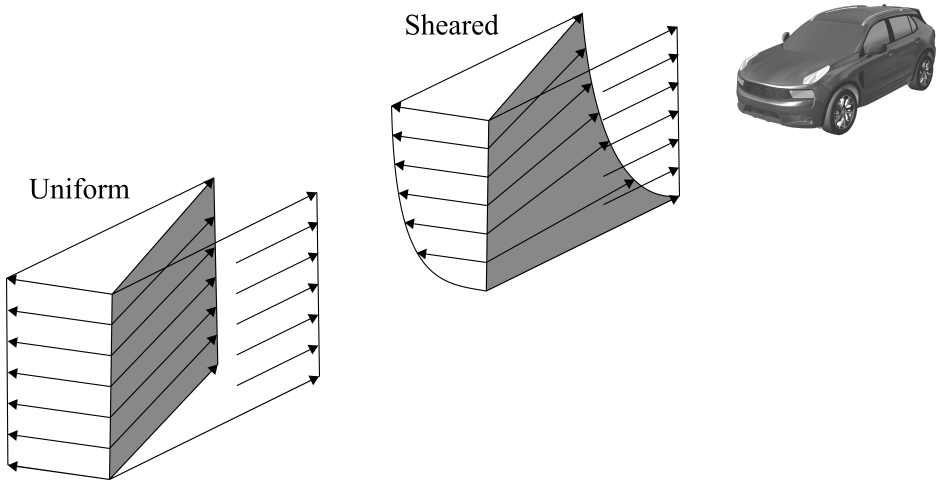

Figure 2.3: *Comparison between the uniform wind and the natural wind, generating the sheared flow (inspired by [5]).*

Wojciak [20] focused on vehicle aerodynamics during crosswind gusts. The first part of [20] focused on quantifying the crosswind gust profiles using a similar wind probe setup as Wordley and Saunders [6]. Wojciak measured the flow conditions during 163 gust events and classified the crosswinds into three different gust profiles. It was also noted that 72 % of the gust events had a zero crossing of the relative incoming flow angle, which was found to have great impact on the aerodynamic response to the crosswind by Theissen [21]. Furthermore, Wojciak showed that the majority of the gust events had peak values of the incoming flow angle of 5 to 9 deg, at a vehicle velocity of 140 km/h, claiming that the ISO21021:2010 [14] uses irrelevant flow angles of over 30 deg.

2.2 Driver behaviour and subjective assessment

When driving on the highway, the driver seeks to correct the vehicle from any lane deviations using the steering. If this becomes difficult or is required too often, it classifies as an issue with driving stability. This section will first review previous work analysing driver behaviour in crosswind conditions. The last part of the section will include a more detailed background on the topic of what is subjectively assessed by the driver as an issue with driving stability.

2.2.1 Driver behaviour

Drivers react differently to crosswind excitations. Nevertheless, a study by Wagner and Wiedemann [25] could conclude that the human driver might amplify the vehicle response when correcting for crosswinds in the frequency range of 0.5 – 2 Hz [25]. At frequencies <0.5 Hz, the driver can correct for the slow changes and at frequencies >2 Hz, the changes are too rapid for the driver reaction [25], and the spectral energy of the flow is also lower at these frequencies [4, 21]. Furthermore, the vortex shedding frequency at the vehicle base is dependent on the flow velocity, but at highway driving it is well above 2 Hz for a typical passenger vehicle [26]. Therefore, it can be assumed that to affect the human-vehicle system in the critical region of 0.5 – 2 Hz external excitations are required, such as crosswinds.

The studies by Wagner and Wiedemann [25] and later Krantz [27] also concluded that a driver, or a representative driver model, should be used to evaluate crosswind sensitivity of the complete system.

2.2.2 Subjective assessment

During vehicle development, the final assessment of driving stability is often done by experienced drivers at test tracks. Their subjective judgement has proven to be reliable and reproducible. However, their subjective evaluation cannot directly be used in any virtual vehicle dynamics computer simulation. Therefore, there is a need to correlate the subjective assessment to objective quantities of the vehicle motion. It has been seen that smaller steering wheel corrections along with low lateral and yaw vehicle response improved the subjective ratings when evaluating the total drivability at high speed [28]. Other studies at crosswind facilities have indicated that the vehicle motions; yaw velocity, lateral acceleration and head-rest acceleration (including roll velocity) give the best correlation to the subjective ratings [10, 29].

2.3 Road vehicle dynamics

The overview of the complete system (Figure 2.1) visualised the interdisciplinary physics applied in this thesis. This section introduces the physics of the dynamic system, starting with describing theory and previous work on vehicle dynamic straight-line handling. Thereafter, the important aspects of crosswind aerodynamics are established followed by a sub-section on simulation techniques and numerical coupling between the two disciplines.

2.3.1 Vehicle dynamic straight-line handling

The lateral tire forces, F_{yt}, determine the road plane dynamics of the vehicle. Lateral tire forces are generated when the wheel's angle differs from its velocity vector. This differing angle (the lateral slip angle, α) is small during normal driving, but can generate high forces depending on the cornering stiffness, C_y. ISO 8855:2011 [30] defines the cornering stiffness as,

$$C_y = -\frac{\partial F_{yt}}{\partial \alpha}. \tag{2.3}$$

Hence, the lateral slip angle multiplied with the cornering stiffness of the tire defines the generated lateral tire force. Furthermore, the cornering stiffness can be combined for each axle (C_f and C_r) and one should note that it is not a constant, since it is affected by the normal load and other varying driving conditions. The balance between front and rear axle cornering stiffness determines how the vehicle rotates (yaw) when a lateral force is applied, i.e. centrifugal force or aerodynamic side force, F_S. At some longitudinal position along the vehicle, the lateral force will not rotate the vehicle in any direction. This can be described as a *cornering stiffness centre* or a neutral steering point (NSP). Figure 2.4 visualises the NSP along with the aerodynamic centre of pressure (CP), the centre of gravity (CoG) and a geometric reference point midway between the axles. If the NSP is located behind the CoG, the centrifugal force would understeer the vehicle in a steady-state cornering scenario. The distance between CoG and NSP, l_s (Equation 2.4), is therefore a measure of the understeering. However, since the cornering stiffness varies during driving, l_s will also vary.

$$l_s = \frac{C_r l_r - C_f l_f}{C_f + C_r} \tag{2.4}$$

By defining the NSP with respect to the fixed geometric reference point, it can be observed that the NSP is not directly dependent on the CoG positioning (l_f or l_r), see derivation in Equation 2.5. It only depends on the axle cornering stiffness balance and the wheel base.

$$l_{\text{NSP}} = l_s - \left(\frac{L}{2} - l_f\right) = \frac{C_r l_r - C_f l_f}{C_f + C_r} + \frac{l_f - l_r}{2} = \frac{C_r - C_f}{C_f + C_r}\frac{L}{2} \tag{2.5}$$

Aerodynamic centre of pressure

Figure 2.4 present the centre of pressure (CP) in front of the NSP. This is typical for a normal passenger vehicle. However, this also implies that the vehicle is *aerodynamically unstable* (any crosswind would work to rotate the vehicle away from the wind, increasing the relative flow angle). Early work on straight-line handling concluded that CP should be located behind CoG (later corrected to behind NSP) [10, 31]. In 1965, Barth [32] suggested stabilising fins at the rear to improve stability of the vehicle by moving CP rearwards towards CoG and NSP. Nevertheless, that might not be a realistic solution and even though the vehicle is aerodynamically unstable, the complete vehicle dynamic system can remain stable due to the road contact. Favre et al. [33] conducted a numerical study where CP, CoG and NSP were altered independently (the NSP position was altered by varying the cornering stiffness, to decouple its influence from the CoG position). As expected, it was concluded that CP should be moved rearward, primarily to decrease the distance to NSP, and that NSP should be located behind the CoG [33].

The aerodynamic forces and moments are often defined in the reference point between the axles [34]. The aerodynamic yaw moment can thus be defined as $M_z = F_S l_{\mathrm{CP}}$. The distance between CP and the reference, l_{CP}, will also vary since the aerodynamic side force, F_S, and yaw moment, M_z, are not strictly linearly dependent. In summary, Figure 2.4 give valuable insights on straight-line handling. Although, as stated above, the positions of NSP and CP move depending on the driving scenario and wind load.

Aerodynamic lift forces

The cornering stiffness increase with the normal load. Therefore, the aerodynamic lift forces at the front and rear axle will affect the cornering stiffness and thus the driving dynamics at high speed. Milliken et al. [35] introduced a static stability index in 1976, based on a bicycle

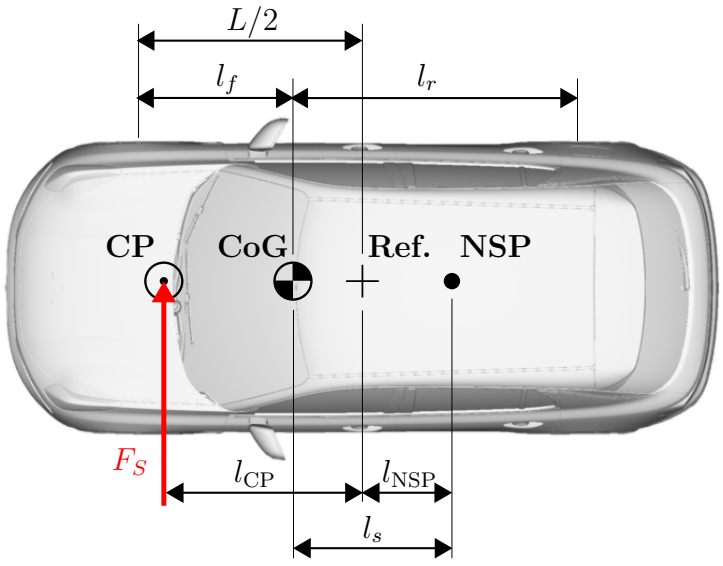

Figure 2.4: *Top view of a vehicle visualising the typical longitudinal positions of the aerodynamic centre of pressure (CP), the centre of gravity (CoG), a geometric reference point between the axles (Ref.) and the neutral steering point (NSP).*

model with linearised tire cornering stiffness. The negative values of the index were defined as stable. It was shown that the value of the index increased with the vehicle velocity, agreeing with the decreased yaw damping at higher velocities (an oversteered vehicle would reach a stability index of zero at its critical velocity). The stability index has been used in parametric studies, showing that a positive lift balance ($C_{lf} - C_{lr}$) increases the stability of the vehicle [36]. This corresponds to decreasing the cornering stiffness at the front axle and increasing it at the rear, moving the NSP further rearward according to Equation 2.5. Howell and Le Good [37, 38] conducted subjective on-road experiments, where test drivers evaluated the high speed stability performance of several vehicles with varying lift force coefficients. The increased stability performance with positive lift balance was confirmed in the study [37].

Vehicle dynamic parameters

The static stability index was further used to highlight important vehicle dynamic properties. It was found beneficial to decrease the yaw mass moment of inertia and especially to move CoG forward, increasing the vehicle understeer [36]. This was also established by MacAdam et al. [10] in 1990 and later in other studies [19, 39, 40]. MacAdam et al. also showed the advantage of moving CP rearward (in agreement with the theory above) and the benefit of increased roll stiffness.

Suspension characteristics

The suspension system controls the relative motion between the wheel and the vehicle body. The wheel motion is determined by the geometrical hardpoints of the linkages in the suspension. The suspension can therefore be designed to create advantageous wheel angles at certain driving scenarios. However, all geometrical suspension designs have benefits and drawbacks and it is up to the engineers to find the best fit for their vehicle and customers. The geometrical motion (kinematics) determined by the hardpoints might generate steering angles during motions of the vehicle body, e.g. heave or roll. These steering angles affect the straight-line stability during crosswinds, where the lateral acceleration and aerodynamic roll moment can cause vehicle roll. Furthermore, the bushing and linkages in the suspension and steering system deform elastically to lateral loads (elasto-kinematics). The crosswind aerodynamics will therefore affect the side force steering of the vehicle. The design of the suspension system can thus be another tool in improving crosswind stability.

2.3.2 Crosswind aerodynamics

The background and theory on aerodynamics will first cover constant crosswind conditions, then transient crosswinds and finally a sub-section covering aerodynamic stability without crosswinds.

Constant crosswinds

Perpendicular crosswinds, w_y, induce flow angles, ψ, relative to the direction of the vehicle, see Figure 2.5. The vehicle velocity, v_x, and wind components, w_x and w_y, affect the resulting flow

angle and magnitude, V_{mag}, as in,

$$V_{\text{mag}} = \sqrt{(v_x + w_x)^2 + w_y^2}, \qquad \psi = \arctan\left(\frac{w_y}{v_x + w_x}\right). \tag{2.6}$$

The aerodynamic forces and moments are determined by the magnitude and angle of the flow. As the vehicle goes faster, the flow angle decreases. Nevertheless, the aerodynamic forces and moments will increase at higher velocities. As shown in Equation 2.7, the aerodynamic side force, F_S, increases exponentially with flow velocity, V_{mag}.

$$F_S = \frac{1}{2}\rho A C_S(\psi) V_{\text{mag}}^2 = K_1 C_S(\psi) V_{\text{mag}}^2 \tag{2.7}$$

The density of air, ρ, and frontal area, A, can be set (together with the half) to the constant K_1 to simplify the expression. The coefficient of side force, C_S, is a function of the incoming flow angle, ψ. So, the forces' and moments' quadratic increase with flow velocity holds for a constant flow angle. However, as the flow angle decreases with increasing vehicle velocity, a more realistic setting for high speed driving is to keep the crosswind velocity, w_y, constant. In this scenario, without head- or tail wind ($w_x = 0$), the flow angle decrease approximately linear with the vehicle velocity. The first approximation in Equation 2.8, that the side force coefficient is directly proportional to the flow angle, was seen for multiple vehicle models in the study by Howell and Panigrahi [41]. This linearization is presented using a constant, K_2. The second approximation of small angles, together with the assumption of Reynolds number independent aerodynamic coefficients, implies that the vehicle velocity is high, e.g. above 100 km/h, which is in the range of interest for high speed driving stability.

$$C_S(\psi) \approx K_2\psi = K_2 \tan^{-1}\left(\frac{w_y}{v_x}\right) \approx K_2\frac{w_y}{v_x} \tag{2.8}$$

The resulting side force expression in Equation 2.9 shows an approximately linear increase with vehicle velocity and crosswind velocity. Hence, doubling the driving speed will almost

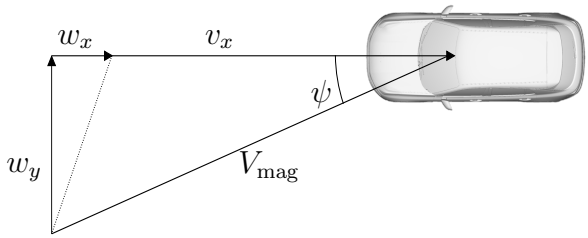

Figure 2.5: *Schematics of how the flow angle, ψ, and flow velocity, V_{mag}, relate to the vehicle velocity, v_x, and horizontal wind components, w_x and w_y.*

double the side force, even though the crosswind velocity is kept constant, see Figure 2.6.

$$\Rightarrow F_S = K_1 K_2 w_y \left(v_x + \frac{w_y^2}{v_x} \right) \tag{2.9}$$

The same approximations can be done for the aerodynamic yaw moment, M_z, (or any aerodynamic coefficient with a linear dependency on the flow angle). In summary, this simplified example shows that the increase in aerodynamic side force and yaw moment occur simultaneously as the yaw dampening of the vehicle is decreasing with increasing speed, making the vehicle more crosswind sensitive at high speeds. These two facts exemplify why high vehicle velocity affects the stability performance of a road vehicle.

Transient crosswinds

So far, this section has discussed aerodynamics in constant crosswind. However, that is a rare on-road condition, as mentioned in Section 2.1. Time-dependent, *transient*, crosswind conditions further intensify the challenges with driving stability. Chadwick et al. [42] could experimentally show high overshoots in the aerodynamic yaw moment when exciting both a sharp-edged and a radiused-edged box to transient crosswinds. Similar results were presented by Theissen [21], were the overshoots in the yaw moment was explained by the delay in flow angle between the front and rear of the vehicle, when driving into crosswinds. It was shown that these effects could not be captured in a quasi-steady aerodynamic model, where the aerodynamic coefficients obtained at constant crosswinds are used.

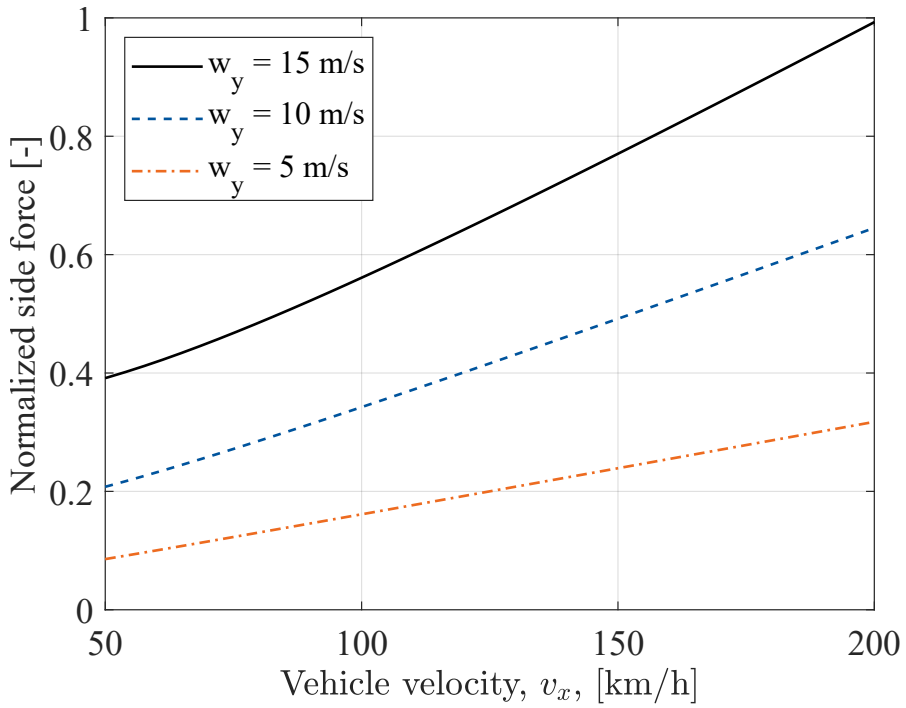

Figure 2.6: *The side force increase with vehicle velocity, v_x, and crosswind velocity, w_y, based on Equation 2.9. Normalised with the side force at* 200 km/h *and* $w_y = 15$ m/s.

The early work on classifying wind conditions was based on wind loading for structures, such as buildings, where an aerodynamic admittance function was used [43]. The aerodynamic admittance (transfer function) describes how the dynamic overshoots of the forces and moments are affected by the frequency of the crosswind flow, compared to the steady crosswind forces [44]. The non-dimensional Strouhal number is often used when analysing oscillating flows. The frequency, f, of the flow is non-dimensionalised by the characteristic length, L_v, and the freestream velocity, V_∞, see Equation 2.10. Stoll and Wiedemann [45] investigated the DrivAer notchback's aerodynamic side force and yaw moment admittance using a transient crosswind windtunnel setup and two simulation methodologies. The results showed side force admittance close to unity (quasi-steady) before a drop-off at St = 0.15. In contrary, the yaw moment admittance showed an increase up until St = 0.15 and thereafter a decrease.

$$\mathrm{St} = \frac{f L_v}{V_\infty} \tag{2.10}$$

Another quantity, related to the Strouhal number, is the reduced frequency [4], see Equation 2.11. A rule-of-thumb is associated with this quantity, where the aerodynamics is defined as steady-state at $K = 0$, quasi-steady when $K < 0.1$ and unsteady when $K > 1.0$ [4]. Note, that the range $K = 0.1$ *to* 1.0 is neither classified as quasi-steady nor unsteady. The spectral energy flow cascade can be seen in Figure 2.7, depending on crosswind frequencies at 160 km/h and corresponding St, K and λ/L_v values. For reference: the critical crosswind scale region

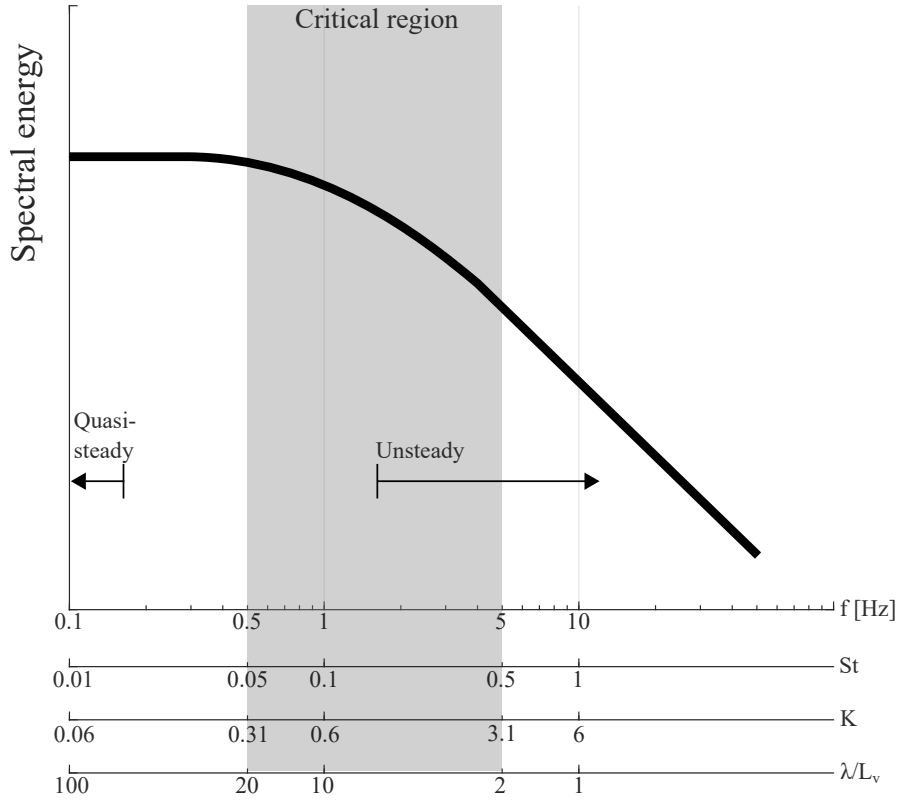

Figure 2.7: *The spectral energy of the crosswind flow and relevant scales for driving stability (inspired by [4] and [20]).*

of 2-20 vehicle lengths, λ/L_v, corresponds to $K = 3.1$ *to* 0.3, respectively. However, it is important to note that this is just a rule-of-thumb. For example, Fuller and Passmore [46] found transient flow effects originating from a-pillar separation of a 1/6 scale Davis model at the reduced frequency of 0.098 (quasi-steady). On the other hand, Oettle et al. [47] found the side window surface pressure develop quickly at crosswind changes and that it could be accurately approximated using a quasi-steady model up to $K = 1.0$.

$$\mathrm{K} = \frac{2\pi f L_v}{V_\infty} = 2\pi\mathrm{St} \tag{2.11}$$

No crosswinds

Most research investigating driving stability performance at high speeds have assumed that the transient flow conditions, such as crosswinds, are the most important load case for investigating straight-line stability. In contrary, a study in 2015 by Kawakami et al. [48] looked at aerodynamic load fluctuations at zero flow angle. The study was performed using LES simulations and scale-model wind tunnel tests. The CFD results showed that small delta-winglets (vortex generators) at the rear lamp and at the side of the roof spoiler could suppress the aerodynamic yaw and roll moment fluctuations at a Strouhal number of 0.1. Experimental flow measurements showed that the shear layer behind the vehicle was reduced with the vortex generators, indicating a more distinct separation line. Finally, a subjective driving assessment was performed by experienced drivers, where the vortex generators increased the stability performance score.

2.3.3 Numerical modelling and simulations

With the recent years' increased capability of simulation power and the improvement of CAE (computer-aided engineering) tools, research on coupling aerodynamic and vehicle dynamics simulations have increased.

Aerodynamic response modelling

The aerodynamic response to a crosswind gust can be modelled or simulated in many ways. Jarlmark [49, 50] and later Juhlin [51, 52] created inverse dynamics models to estimate the aerodynamic load on the vehicles while driving on roads. This was done by measuring the wind, the motion of the vehicle and the driver response. The inverse simulations could thus enable an approximate solution without using full-scale windtunnels with crosswind excitation abilities. A few studies have been performed at such facilities [45, 53]. However, since crosswind windtunnels are rare, much research has been focused on using computational fluid dynamics (CFD) simulations to model the transient aerodynamic loads during the crosswind gust events [12, 13, 15–19, 54].

Vehicle dynamic response modelling

The vehicle dynamic models' level of fidelity varies in the studies analysing crosswind stability. Some studies have implemented the classical one-track *bicycle* model, which has 2 degrees of freedom (lateral and yaw motion) [16, 55]. Other studies have opted for more advanced analytical model, sometimes incorporating two tracks with vertical degree of freedom, roll

Table 2.1: *List of studies coupling aerodynamics and vehicle dynamics. The vehicle geometry, aerodynamic modelling method, vehicle dynamic model fidelity and coupling method are stated.*

Year	Authors	Vehicle	Aerodynamics	Vehicle dynamics	Coupling
2020	Tunay et al.[19]	Bus	CFD	Advanced	2-way
2019	Huang et al.[18]	Sedan	CFD	MBD	2-way
2018	Li et al.[17]	Sedan	CFD	MBD	2-way
2017	Huang et al.[57]	Sedan	CFD	Advanced	2-way
2017	Lewington et al.[13]	3 Fords	CFD	MBD	1-way
2017	Nakasato et al.[12]	Hatchback	CFD	MBD	2-way
2016	Favre et al.[33]	Windsor	CFD	Advanced	1-way
2016	Forbes et al.[15]	DrivAer	CFD	Advanced	2-way
2016	Carbonne et al.[16]	Windsor/bus	CFD	Bicycle	2-way
2016	Winkler et al.[55]	Bus	CFD	Bicycle	2-way
2013	Nakashima et al.[56]	Truck	CFD	Advanced	2-way
2010	Nakashima et al.[58]	Truck	CFD	Advanced	1-way
2008	Juhlin[51]	Bus	Inverse	Real/MBD	Real
2002	Jarlmark[49]	Volvo	Inverse	Real/MBD	Real

dynamics and more detailed steering system and suspension models [15, 19, 33, 56–58]. To further increase the accuracy, high-fidelity multi-body dynamic (MBD) models are needed. Several studies have used these MBD models when simulating the coupled aerodynamic and vehicle dynamic response [12, 13, 17, 18], see Table 2.1.

Aerodynamic and vehicle dynamic numerical coupling

The straightforward coupling method would be to simulate the aerodynamic forces separately and apply them to the vehicle dynamic model, as in a one-way coupling. However, as shown at the beginning of the chapter (Figure 2.1), the orientation of the vehicle affect the relative flow conditions and thus the aerodynamics. Therefore, a more authentic (but more computationally expensive) description would be to simultaneously account for the vehicle dynamic motion response in the aerodynamic simulation, creating a two-way coupling. Some studies suggest that a one-way coupling is sufficiently accurate for passenger vehicles [15, 16], while another study opted for the necessity of a two-way coupling [18]. Higher vehicles (buses and trucks) show a greater discrepancy between the coupling methods indicating that the one-way coupling is insufficient for large vehicles [16, 56]. Table 2.1 show previous studies coupling aerodynamics and vehicle dynamics.

2.4 Vehicle development process

As discussed, when developing a new vehicle, the evaluation of driving stability at high speeds is often done subjectively using prototype vehicles, only available at late stages when changes are costly. Issues with driving stability are therefore difficult to deal with and it can be challenging to find balanced compromises for improving driving stability, since this can affect other vehicle attributes. One method of handling this is to set suitable engineering requirements that minimise the risk of developing prototype vehicles with driving stability

issues. These requirements can be used earlier during the design of the vehicle. A common aerodynamic requirement is to limit the balance and sum of the lift coefficients, as the example in Equation 2.12 (from [37]).

$$\begin{aligned} C_L = (C_{lf} + C_{lr}) &\leq 0.20 \\ |C_{lf} - C_{lr}| &\leq 0.10 \end{aligned} \tag{2.12}$$

However, in general, it is difficult to find suitable requirements that work in all vehicle projects with varying suspension systems and other vehicle attributes. An additional method is to move the assessment from the on-road testing at the test tracks to the virtual world, using numerical tools and driving simulators. This has received increased interest during the last decades, with the improvements in computational performance. A virtual assessment of driving stability can also be used in early design phases, enabling improvements when the cost of change is lower and removing most issues before the prototype vehicles are built. However, it is expected that the final evaluation still needs to be done at the test tracks and on real roads.

3

Experimental study on driving stability

An on-road experimental study at a test track was performed with the objective of correlating the drivers' subjective perceptions of driving stability to quantitative measures, at high speeds. In addition, the study was conducted to find realistic aerodynamic load cases for high speed driving stability. This chapter describes the experimental setup and presents the most important results from Paper A.

3.1 Experimental setup

This section describes the setup for the experimental testing at the Hällered Proving Ground and the post-processing of the data. The testing was conducted during a six week period with different wind conditions throughout the weeks. All tests were performed on test tracks in dry conditions and all driving was done by experienced drivers.

3.1.1 Instrumentation

The instrumentation setup was designed to enable synchronised data acquisition of the relative flow conditions, the dynamic motion of the vehicle and the subjective input from the drivers. Table 3.1 lists the measurements and associated equipment.

The local flow magnitude and angle subjected to the vehicle were measured using a 7 hole probe positioned 371 mm above the roof by a probe holder mounted in place of the shark fin antenna, see Figure 3.1. This, to decrease the vehicle's influence on the measured flow and to reduce the flow disturbance over the rear roof spoiler. The probe had a flow cone angle of receptivity of

Table 3.1: *Instrumentation setup for the experimental high speed driving.*

Equipment	Measurement
7-hole probe Prandtl tube	Flow magnitude and angle
Subjective trigger	Instability events
GPS-RTK	Positioning and speed
IMU	Vehicle motion response

70 deg and an accuracy of ±1 deg [59]. The probe's pressure tubes were connected to pressure sensors sampling at 2500 Hz. The pressure sensors measured the pressure difference between a reference pressure (atmospheric pressure) and the holes at the tip of the 7 hole probe. The atmospheric pressure was obtained by the static pressure port of a Prandtl tube mounted 80 mm above the 7 hole probe, see Figure 3.1. The flow magnitude, V_{mag}, and angle, ψ, was calculated using the probe's calibration map with the port pressures as the input. The static port pressure of Prandtl tubes is slightly affected by yawed flow, but the pressure error was assumed to be <2 % for flow angles below 10 deg according to [60]. This did not affect the flow angle calibration only the slight variation in the flow magnitude calibration.

To enable analysis of short events where stability issues were noted, a subjective trigger was installed in the cabin. The button on the trigger could be pressed by the driver while driving, generating a time mark in the data.

Two GPS antennas were mounted inside the vehicle, on the centre line at the wind shield and at the rear of the vehicle. The GPS positioning was enhanced by a real-time kinematic (RTK) system, giving a positioning accuracy of ±0.01 m and velocity accuracy of ±0.1 m/s [61]. The motion of the vehicle was measured using a Dewesoft DS-IMU2 module, an inertial measurement unit (IMU) that combines gyroscopes and accelerometers with measurement accuracies of ±0.033 deg/s and ±0.032 m/s^2, respectively [61]. The IMU was firmly mounted to the structure of the vehicle, close to the centre of gravity (CoG), see Figure 3.1. The acceleration measurements could be translated to any point in reference to the IMU placement. In this study, the lower back of the seated driver was used as a reference point. This reference point was selected to enable correlations between the drivers' subjective assessment and their experienced motion in the vehicle.

3.1.2 Test track and test procedure

An oval test track with two 1.1 km straight runs was used for the high speed testing at Hällered Proving Ground (see Figure 3.2). Three experienced drivers participated in the study. Before the data acquisition, a co-driving session was conducted where all drivers independently could trigger at events of substantial stability issues. As all drivers marked the same events, it was

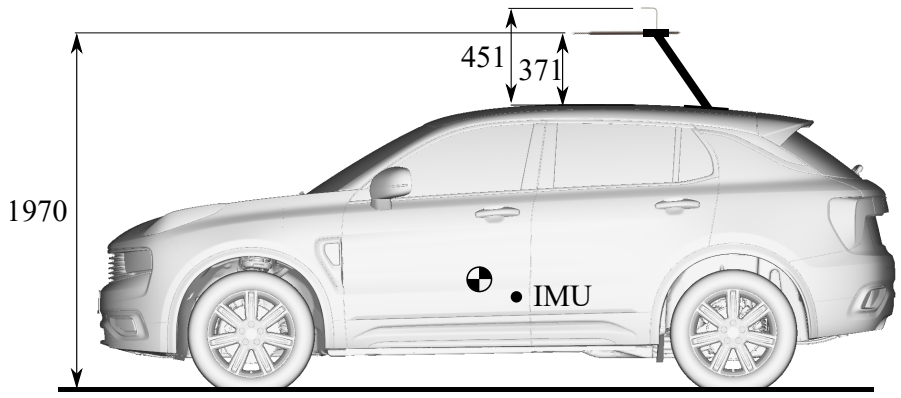

Figure 3.1: *Schematics of the placement of the 7 hole probe and the Prandtl tube in* mm *and the position of the inertial measurement unit (IMU).*

concluded that the data from all three drivers could be used in the study. The data acquisition was automated using GPS locations for starting and stopping the sampling at the beginning and end of the two straights.

The test drivers were instructed to drive in a straight line and to keep the steering wheel fixed. The test procedure started by driving a couple of laps on the test track to verify the functionality of the measurement equipment and to ensure that the tires reached operational temperature. The testing was then conducted at four different velocities; 140 km/h, 155 km/h, 170 km/h and 185 km/h. Each velocity was held constant for three runs at each of the two straights, before changing velocity. To ensure significant results in an environment of uncontrolled repeatability, a large data set of 407 straight line recordings (448 km) were collected, including 255 subjective trigger events.

3.1.3 Post-processing

The flow and vehicle motion data were analysed at the subjective trigger events and compared with the complete data set to find any exceptional trends prior to a trigger. All data were filtered through a Hamming low pass filter of order 500 with a cut-off frequency of 5 Hz. Higher frequencies of the wind and vehicle motion were disregarded for the driving stability analysis.

Subjective trigger event analysis

The time marks from the drivers' subjective triggers were used to analyse the data before the trigger events. Figure 3.3 visualises four signals to exemplify the data analysis with two trigger events as red vertical lines. A window of 3 s before each trigger was marked as the region of instability. It was assumed that the cause of the subjective perception of stability issues would be found within these time intervals, both in terms of the vehicle motion response and crosswind conditions.

Figure 3.2: *An aerial view of Hällered Proving Ground, showing the oval test track (courtesy of Volvo Car Corporation) [62].*

The most robust and useful way to analyse the data was by measuring the amplitude between maximum and minimum peaks within the regions of instability, see Δ amplitudes in Figure 3.3. This was done both for the air flow measurements, to determine typical crosswind conditions before the subjective triggers and for the motion responses experienced by the drivers, to correlate their subjective assessment to quantitative objective measures. The amplitude (peak-to-peak) values were then sorted into intervals to present the distribution of their frequency of occurrence.

All data analysis

The data at the subjective trigger events were compared to the complete data set, to find unusual trends in the trigger data. The comparisons were made using a similar analysis methodology for the complete data set. A sliding window of 3 s, with 1 s stepping, was applied to all the data. Similarly, the maximum amplitude difference between peaks was measured at each step. The amplitude values were then sorted into intervals to present the distribution of their frequency of occurrence, so that it could be compared to the trigger data.

3.2 Results and discussion

The results from the tests are first presented in terms of the environmental wind conditions of interest for driving stability. Thereafter, a section on subjective assessment and correlated objective measures will follow.

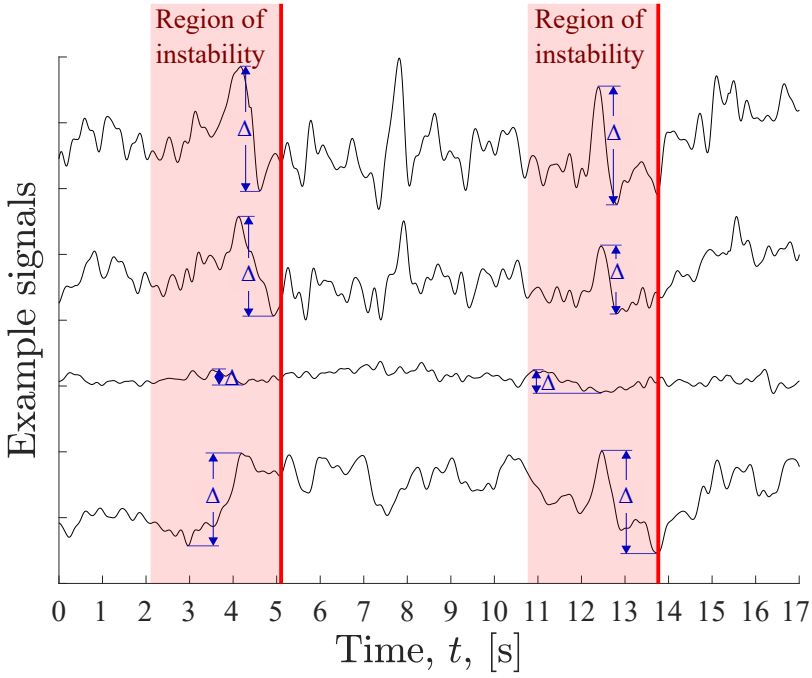

Figure 3.3: *Example of trigger events (red lines) and windows used for the visualisation of the regions of instability.*

3.2.1 Wind load conditions and gust profiles

The data from the test track experiments showed that the vehicle was subjected to crosswinds which mainly varied between 0 to 3 on the Beaufort wind scale, corresponding to wind changes between 0 – 5.4 m/s within a 3 s window, see *All data* in Table 3.2. It is also evident from the table that higher changes in crosswind correlated with a higher fraction of subjective triggers. These distributions are also presented in Figure 3.4a, where the dark brown colour represents the overlap between the two data sets. The discrepancy between the crosswind conditions at the triggers and the complete data set indicates that change in crosswind was an underlying factor for issues with high speed stability performance in this study. Half of all triggers occur in crosswinds with level 4 (5.5 m/s) or above on the Beaufort scale, which only represents 14 % of the total wind data. This correlates a varying crosswind with decreased driving stability performance. However, it should be noted that 16 % of the triggers occur in conditions with no or little wind (0, 1 & 2 on the Beaufort scale). It must, therefore, be assumed that driving stability issues might occur without any crosswind, even though these results show that the majority of the instabilities occur in changing crosswind conditions.

The resulting relative flow angle, ψ, is dependent on the vehicle speed, v_x, and the wind components, w_x and w_y, as presented in Figure 2.5 and Equation 2.6. When driving at 140 km/h without any head- or tailwind, a change in crosswind of 7 m/s results in a relative

Table 3.2: *The frequency of occurrence for triggers and the complete data set, in intervals on the crosswind change corresponding to levels on the Beaufort scale.*

Gust conditions		Percentage	
Beaufort scale	Side wind change, Δw_y, [m/s]	Triggers	All data
0, 1 & 2	0 – 3.3	16 %	42 %
3	3.4 – 5.4	35 %	44 %
4	5.5 – 7.9	41 %	12 %
5	8.0 – 10.7	7 %	2 %
6	10.8 – 13.3	1 %	0 %
		100 %	100 %

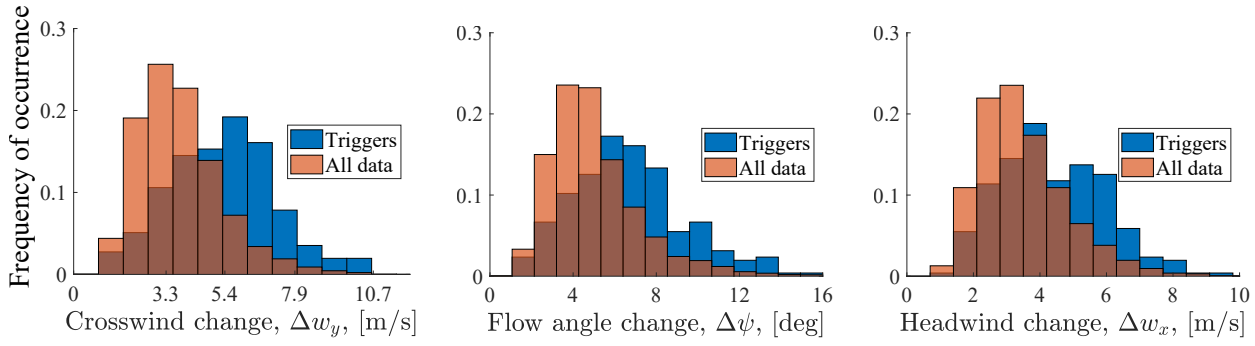

(a) **(b)** **(c)**

Figure 3.4: *The frequency of occurrence distributions for three wind quantities, comparing the data at the trigger events to the complete data set.*

flow angle change of 10 deg. Figure 3.4b shows the flow angle change before the triggers and the distribution for the complete data set. It is evident that the figure display overlapping information with Figure 3.4a. However, since the test procedure included different vehicle velocities the resulting flow angles could be of interest, at least for comparison with other studies. Only one-fourth of the complete data set had a varying flow angle above 6 deg, but 59 % of the triggers were recorded at these flow conditions. Furthermore, gusts above 10 deg were rare, but had a high correlation with stability issues. The distributions presented in Figure 3.4b show a smaller discrepancy between triggers and all data than the crosswind magnitude in Figure 3.4a. The change in crosswind magnitude was, thus, the more relevant measure, of the two different lateral flow quantities.

Figure 3.4c presents the distribution for the change in headwind, Δw_x. Although the discrepancy between the trigger data and the complete data set was small, a change in magnitude above 5 m/s showed an increased occurrence of subjective trigger events. Of course, any crosswind non-perpendicular to the vehicle path would give a reading on the headwind measurements. Hence, one could argue that the change in headwind, Δw_x, and flow angle, $\Delta\psi$, were the indirect effects of stability issues, while the change in crosswind, Δw_y, was the direct effect.

Gust profile formulation

Since the natural wind is turbulent and highly stochastic, none of the crosswind gusts measured at the trigger events were identical. Nevertheless, certain patterns could be observed and a broad classification was done in terms of gust profiles. To enable adoption in numerical flow simulations, the profiles were defined mathematically by a piecewise function of crosswind gust, inspired by Favre and Efraimsson [63]. The function can be seen in Equation 3.1 and has four parameters controlling the crosswind amplitude and four parameters specifying the time duration in each stage of the gust profile, see Figure 3.5 for graphical explanation of the gust parameters.

$$
w_y(t) \begin{cases}
= \boldsymbol{w_y^{\text{start}}} & \text{for } t < t_0 \\
= \boldsymbol{w_y^{\text{start}}} + \frac{\boldsymbol{w_y^{\max}} - \boldsymbol{w_y^{\text{start}}}}{\boldsymbol{2}} \left(\boldsymbol{1} - \boldsymbol{\cos}\left(\frac{\boldsymbol{\pi}}{\boldsymbol{t_b}} \left(\boldsymbol{t} - \boldsymbol{t_0}\right)\right)\right) & \text{for } t_0 < t < t_0 + t_b \\
= \boldsymbol{w_y^{\max}} & \text{for } t_0 + t_b < t < t_0 + t_b + t_p \\
= \boldsymbol{w_y^{\max}} - \frac{\boldsymbol{w_y^{\max}} - \boldsymbol{w_y^{\min}}}{\boldsymbol{2}} \left(\boldsymbol{1} - \boldsymbol{\cos}\left(\frac{\boldsymbol{\pi}}{\boldsymbol{t_d}} \left(\boldsymbol{t} - \boldsymbol{t_0} - \boldsymbol{t_b} - \boldsymbol{t_p}\right)\right)\right) & \text{for } t_0 + t_b + t_p < t < t_0 + t_b + t_p + t_d \\
= \boldsymbol{w_y^{\min}} & \text{for } t_0 + t_b + t_p + t_d < t < t_0 + t_b + 2t_p + t_d \\
= \boldsymbol{w_y^{\text{end}}} + \frac{\boldsymbol{w_y^{\min}} - \boldsymbol{w_y^{\text{end}}}}{\boldsymbol{2}} \left(\boldsymbol{1} + \boldsymbol{\cos}\left(\frac{\boldsymbol{\pi}}{\boldsymbol{t_b}} \left(\boldsymbol{t} - \boldsymbol{t_0} - \boldsymbol{t_b} - \boldsymbol{2t_p} - \boldsymbol{t_d}\right)\right)\right) & \text{for } t_0 + t_b + 2t_p + t_d < t < t_0 + 2t_b + 2t_p + t_d \\
= \boldsymbol{w_y^{\text{end}}} & \text{for } t > t_0 + 2t_b + 2t_p + t_d
\end{cases} \tag{3.1}
$$

All gusts in proximity to the subjective event triggers with crosswind variations above 3 on the Beaufort scale were visually inspected and classified into four profiles (A-D). The profiles and their occurrence percentage can be seen in Figure 3.6.

A is characterised by a continuously changing crosswind, with a zero-crossing between two peak values. This type of crosswind gusts was one of the most frequent in the experimental data. The regularly changing crosswind implies that the drop time is longer than the build-up time, $t_d > t_b$.

B is characterised by a slow build-up time and a rapid drop including a zero-crossing. This quick change, including a zero-crossing was often noted by the drivers to cause substantial stability issues. The profile is similar to profile A, except that the drop time is shorter than the build-up time, $t_d < t_b$.

C is characterised by the quick ramp-up and ramp-down of the crosswind and a relatively long pause at the maximum crosswind magnitude without any zero-crossing. The gust profile starts and ends with no crosswind and is the profile that best represents the crosswind sensitivity testing at crosswind facilities, described in ISO 12021:2010 [14]. This type of crosswind was however the least common during the experimental on-road testing at the test track.

D is characterised by a simple transition between two levels in the magnitude of the crosswind. The example in Figure 3.6 includes a zero-crossing, but the experimental data also showed examples of a quick ramp down from a constant crosswind to no crosswind. The build-up and pause times are set to zero in this profile, $t_b = t_p = 0$, and the initial crosswind magnitude equals the maximum magnitude, $w_y^{\text{start}} = w_y^{\text{max}}$, and the end and minimum magnitudes are also equal, $w_y^{\text{min}} = w_y^{\text{end}}$. A step function of the crosswind can be created by decreasing the drop time duration towards zero, $t_d \to 0$.

Profiles A and B can be seen as variants of a common base profile and that their combined percentage was 35.7 %. However, it is evident that the wind data were highly irregular since

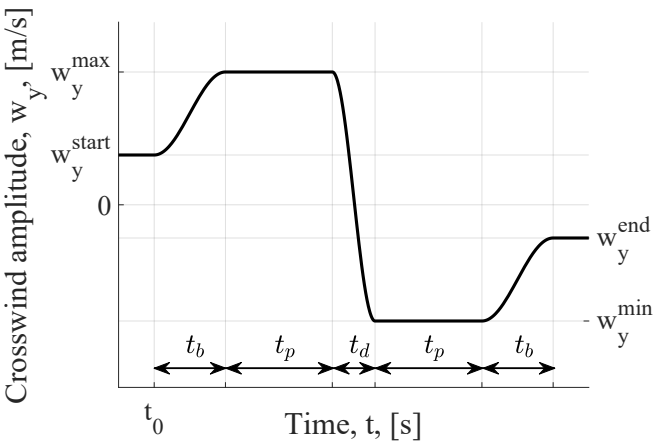

Figure 3.5: *Graphical representation of the gust parameters in Equation 3.1, were the time parameters define the build-up time, t_b, pausing time, t_p and the drop time t_d.*

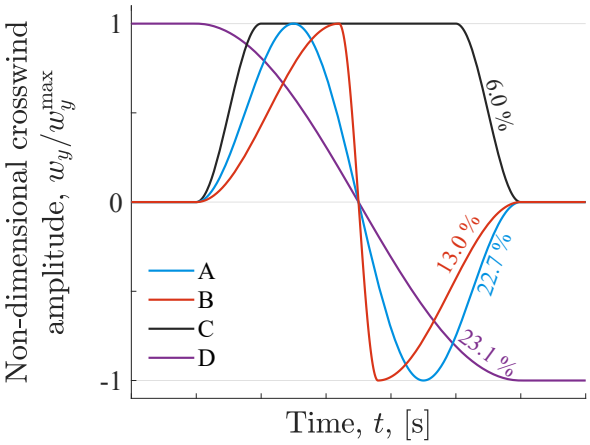

Figure 3.6: *The four gust profiles (A-D) classified in the experimental study and their frequency of occurrence (35.2 % undefined).*

35.2 % of the crosswind gusts did not fit into any of the four profiles. Nevertheless, this classification of gust profiles enhances the possibility to use real-world inspired crosswind gust profiles in virtual simulations.

3.2.2 Objective assessment

The motion response data of the test vehicle was used to correlate the drivers' subjective assessment with certain vehicle motion, to formulate an objective measure for driving stability performance. Figure 3.7a shows the frequency of occurrence distribution for the change in longitudinal acceleration, Δa_x, during 3 s windows of the complete data set compared with the data prior to trigger events. 60 % of all data lies in the interval of 0.1 – 0.2 m/s^2, which was also the case for the trigger data. However, a small discrepancy between trigger data and the complete data set can be seen indicating that a trigger was more frequent when the change in longitudinal acceleration was $\geq$0.2 m/s^2.

In general, the change in lateral acceleration, Δa_y, proved to be greater compared to the longitudinal acceleration, note the x-axis limits in Figure 3.7b. Hence, the driver is subjected to higher variations in lateral acceleration at normal straight-line driving. More interestingly, the discrepancy between trigger data and the complete data set was greater for the lateral acceleration, indicating that this vehicle motion can be correlated to the driving stability performance. For example, only 36 % of the complete data had magnitude variations above 0.5 m/s^2 while the number was 75 % for the data at the trigger events.

The yaw velocity, ω_z, and lateral acceleration, a_y, are motions in the road plane and will later

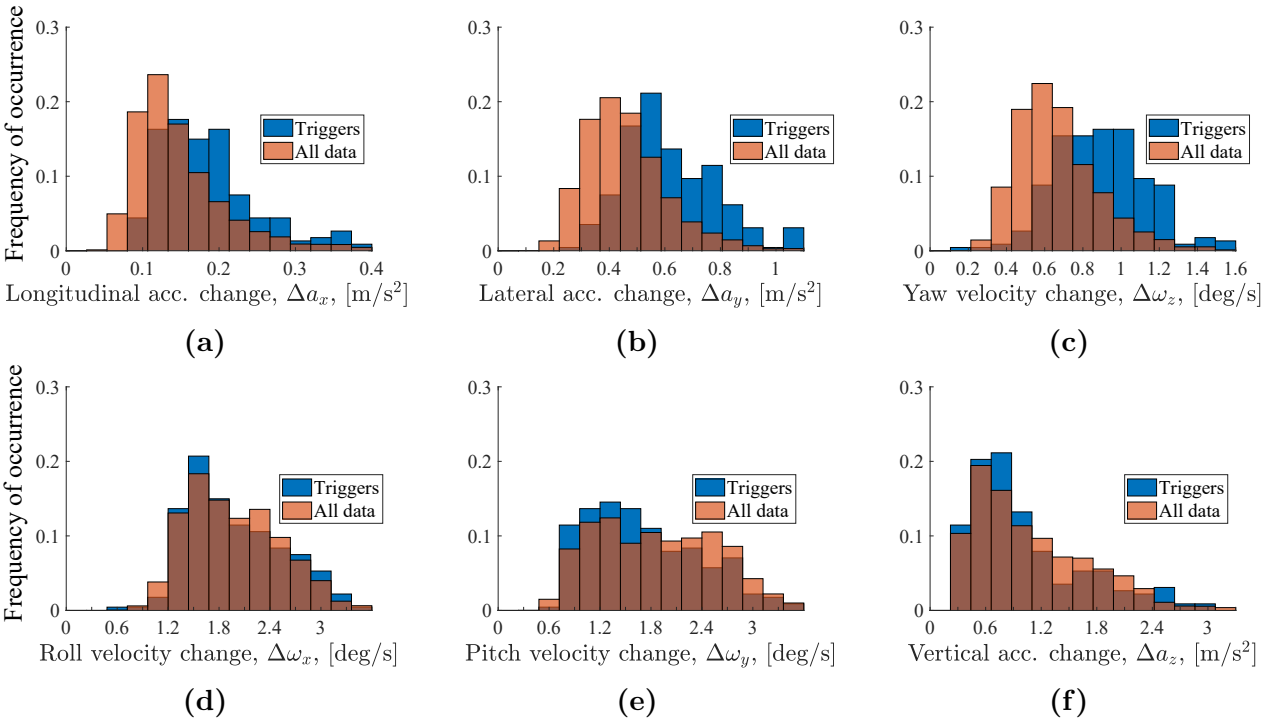

Figure 3.7: *The probability of occurrence distributions for six vehicle motion quantities, comparing the data at the trigger events to the complete data set.*

be shown to have a high correlation between themselves. Figure 3.7c show that there was an even larger discrepancy between triggers and all data for the change in yaw velocity, $\Delta\omega_z$, where 33 % of the trigger data varies >1.0 deg/s (compared to only 8 % of the complete data set).

The roll velocity, ω_x, pitch velocity, ω_y, and vertical acceleration, a_z, had higher variations at normal straight-line driving compared to yaw velocity, longitudinal and lateral acceleration. According to Figure 3.7d, the change in roll velocity, $\Delta\omega_x$, had almost no discrepancy between trigger data and the complete data set. Hence, it could be concluded, using this analysis method, that large changes in roll velocity were not the cause for the drivers' subjective triggers. Similarly, no discrepancies could be seen for either the change in pitch velocity, $\Delta\omega_y$, or vertical acceleration, Δa_z, see Figures 3.7e and 3.7f. Consequently, even though the roll velocity, pitch velocity, and vertical acceleration generally had higher magnitude variations compared to the other three vehicle motions, they did not correlate with poor high speed stability performance. The oscillating vibrations from the road are expected by the driver and were thus not evaluated as something exceptional.

In summary, high changes in lateral acceleration and yaw velocity both seem to correlate with lower driving stability performance. The amplitude changes of these vehicle motion responses were combined to formulate a proxy measure for the stability performance. The combined measure utilises an elliptic formulation of the amplitudes, see Equation 3.2, where Δa_y and $\Delta\omega_z$ were the configuration's amplitude measure for lateral acceleration and yaw velocity, respectively. Note that the units in Equation 3.2 should be [m/s^2] in Δa_y , [deg/s] in $\Delta\omega_z$ and that the formula is not claimed to be general for any driving.

$$Y = \sqrt{2\left(\Delta a_y\right)^2 + \left(\Delta\omega_z\right)^2} \tag{3.2}$$

Figure 3.8 show the amplitude responses of the complete data set together with the combined

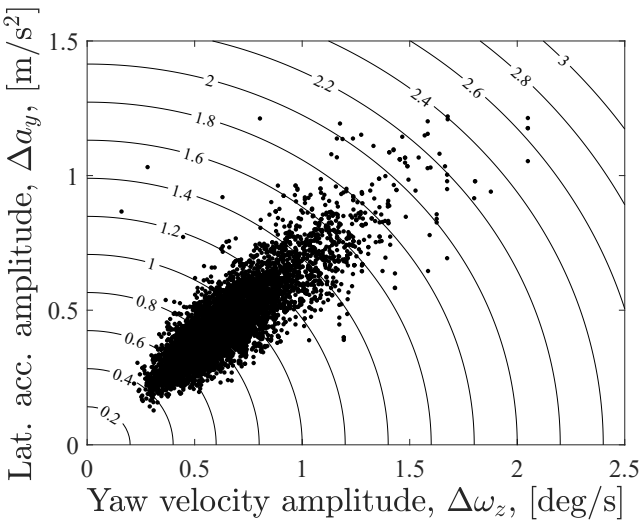

Figure 3.8: *The response amplitudes for the complete data set, with the objective measure (Equation 3.2) visualised as contour lines.*

objective measure. The axes show the amplitude measures while the contour lines indicate the value of the objective measure calculated using Equation 3.2. The figure also shows the strong correlation between lateral acceleration and yaw velocity, but the measure is designed to promote a low response for both vehicle motions.

4

Numerical crosswind stability modelling

The experimental results presented in the previous chapter provided valuable information on realistic aerodynamic load cases along with an objective proxy measure for driving stability. This chapter builds on this knowledge and presents the numerical study from Paper B, intending to find appropriate virtual tools for assessing crosswind stability and to gain insights of the physical coupling between aerodynamics and vehicle dynamics.

The numerical study was conducted at the fixed vehicle velocity of 160 km/h.

Table 4.1: *Numerical crosswind gust profile parameter values applied in Equation 3.1.*

	w_y^{start} [m/s]	w_y^{max} [m/s]	w_y^{min} [m/s]	w_y^{end} [m/s]	t_b [s]	t_p [s]	t_d [s]	$t_{\text{gust}} = 2t_b + 2t_p + t_d$ [s]
Profile 1	0	5	-5	0	0.5	0	0.6	1.6
Profile 2	0	5	-5	0	0.7	0	0.2	1.6
Profile 3	0	5	5	0	0.3	0.5	0	1.6

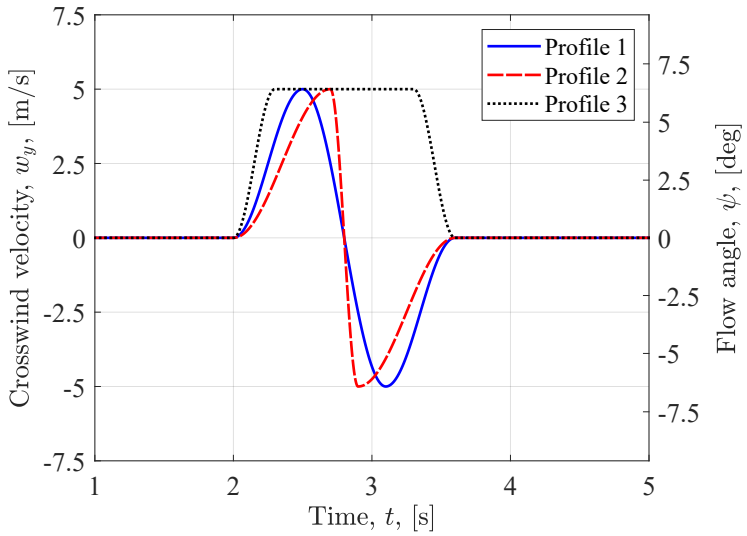

Figure 4.1: *The three numerical crosswind gust profile velocities, w_y, and corresponding flow angles, ψ, at* 160 km/h.

4.1 Aerodynamic methodology

The crosswind gust classification derived in the experimental study (Figure 3.6) was used to formulate three gust profiles in the numerical study. Profiles 1, 2 and 3 corresponded to gust class A, B and C, respectively, see Table 4.1 and Figure 4.1. The crosswind amplitude of $\pm 5\,\mathrm{m/s}$ was at the upper limit of what was seen during the experimental testing (Figure 3.4a) and was chosen to generate high aerodynamic forces within the observed wind conditions. This corresponds to a flow angle change of $\pm 6.4\,\mathrm{deg}$ at the vehicle velocity of $160\,\mathrm{km/h}$. The gust duration, t_{gust}, of $1.6\,\mathrm{s}$ was chosen based on typical gusts seen in the experimental data. It corresponds to 16 vehicle lengths, which lies in the critical range for vehicle dynamic crosswind stability reported in previous works [4, 20, 21]. Profile 1 and 2 were chosen for investigating the effects of different build-up times, t_b, and drop times, t_d, for gust profiles including a zero-crossing of the flow angle. The third profile does not include the zero-crossing, but has a fast build-up time and longer pausing time, t_p, and thus a higher integral of the crosswind velocity.

The aerodynamic forces and moments were defined on the centre-line midway between the axles at ground level, according to [34]. The transient aerodynamic forces caused by the crosswind gust profiles were modelled or simulated using three methods:

1. A **Quasi-steady (QS)** approach; uses tabled data of time-averaged aerodynamic loads at a range of set flow angles to create a linear interpolant. The averaged data originated from unsteady CFD simulations at constant flow angles. The interpolant function determines the aerodynamic response during the crosswind gust, based on the instantaneous flow angle and magnitude. This method is flexible since the aerodynamic load from any gust profile can be approximated once the tabulated data is created (within the flow angles of the tabulated data). The drawback is that all transient aerodynamic effects are neglected.

2. A **Quasi-steady with axle delay (QSD)** approach; extends QS by accounting for the effect of the time delay between the front and rear axle when driving into a gust ($\Delta t = \frac{L}{v_x}$). This is one way to represent the flow delay along the vehicle. The yaw moment and side force were split up into front and rear side forces, as

$$F_{sf} = \frac{F_S}{2} + \frac{M_z}{L} \text{ and} \tag{4.1}$$

$$F_{sr} = \frac{F_S}{2} - \frac{M_z}{L}. \tag{4.2}$$

Similarly, the lift force and pitch moment were split up into front and rear lift. The roll contribution was split equally between the axles. This per-axle formulation enabled the phase shift of the aerodynamic response, e.g. the side force yaw moment:

$$F_S(t) = F_{sf}(t) + F_{sr}(t - \Delta t) \tag{4.3}$$

$$M_z(t) = \frac{L}{2}\left(F_{sf}(t) - F_{sr}(t - \Delta t)\right) \tag{4.4}$$

The QSD has the same advantages as the QS with the addition of accounting for the transient aerodynamic effect of the axle delay. However, the method neglects any transient fluid dynamic effects.

3. A **transient CFD (tCFD)** approach; simulates the full crosswind gust events twice via a transient inlet condition. Each gust was simulated twice (with different starting times of the gust) to increase the reliability of the transient solution by making an average of the forces and moments at each time step. This approach accounts for the axle delay and any fluid dynamic effects, but require two simulations per gust profile making it costly.

The same computational domain was used for generating the tabulated data for the quasi-steady approaches and the transient CFD approach. The domain can be seen in Figure 4.2a. The tCFD approach had a user-defined time-dependent inlet condition for the crosswind velocity while the quasi-steady approaches had constant values. The gusts were transported through the domain by the inlet velocity and the periodic side boundaries. The pressure outlet can be seen to the right and the top of the domain used a symmetry boundary condition. The ground was modelled by a moving wall boundary condition of the vehicle velocity of 160 km/h and the wheel rotation was modelled using a rotating wall boundary condition.

The CFD mesh was adapted for crosswind simulations, by widening the refinement zones aft the vehicle. The prism layer creation was done adaptively by the solver. The adaption was based on the flow around the vehicle in a steady-state solution at zero flow angle. The boundary cells were split until the target of $y^+ < 1$ was reached. This resulted in an average of 17 prism layers on the exterior and a final mesh of 200 million cells. Two views of the final mesh can be seen in Figures 4.2b and 4.2c. The same mesh was used for all aerodynamic modelling approaches.

All simulations were performed using the stress-blended eddy simulation (SBES) turbulence model [64] in the commercial finite volume solver ANSYS Fluent 2020R1. The SBES model is designed with a stronger shielding of the RANS region and a faster transition to the LES region, compared with other DES models, making it more accurate for separating flows [64]. The time step size was set to 2.5×10^{-4} s, corresponding to a temporal resolution of 406 time steps of the freestream to travel the length of the vehicle. A study by Ekman et al. [65] found this resolution adequate when using the SBES model. The same numerical solver settings were used for all aerodynamic modelling approaches.

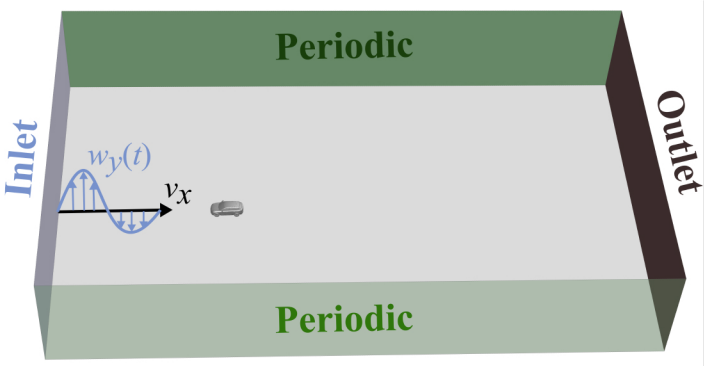

(a) *The computational domain.*

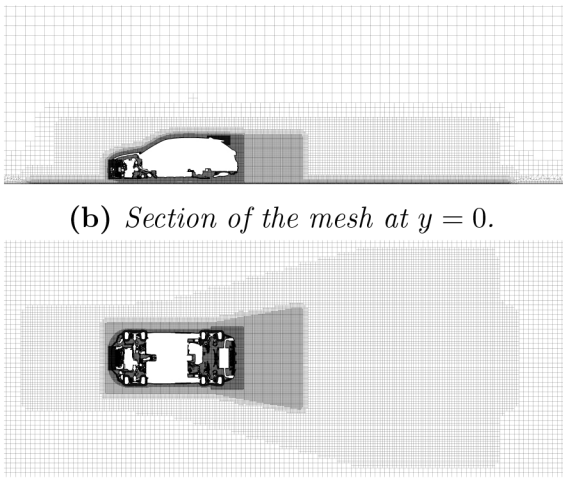

(b) *Section of the mesh at* $y = 0$.

(c) *Section of the mesh at axle height.*

Figure 4.2: *The CFD domain and mesh setup.*

4.2 Vehicle dynamic methodology

Vehicle dynamic models are used to enable virtual assessment of vehicle response in various driving scenarios. The models must, therefore, be representative of the real vehicle and have sufficient fidelity (accuracy) to emulate the vehicle response. The most accurate models are the detailed multi-body dynamics (MBD) models, where kinematic and elasto-kinematic effects of the chassis, suspension and steering systems are modelled as one complex system. As a result, the MBD models use the suspension and steering components' positions (hardpoints) as input for building the model; thus, defining the model on a low hierarchical level. These complex models are often said to be of high fidelity. However, due to their complexity, high-fidelity models can be more difficult to interpret than models of lower fidelity. Moreover, vehicle requirements are set on a system level, a higher hierarchy compared to the hardpoint defined models. Hence, this becomes a drawback when trying to analyse the sensitivity of system properties, since multiple properties change when altering the hardpoints in the high-fidelity models. A viable alternative is to use the models defined on a system level, such as the bicycle model. Although they present lower fidelity, their inherent definition makes them useful when assessing system properties and finding suitable requirement settings. Additionally, the models of lower fidelity are generally more interpretable, giving more insight in the dynamics of the system, and can be used earlier in the vehicle design process when hardpoint details are still not defined. Despite their many advantages, when lower fidelity models are preferred, the issue of accuracy still needs to be addressed.

The accuracy of the lower fidelity models must be balanced with their complexity. Too little detail and the models cannot emulate the correct vehicle response anymore. Too much detail and the models lose their interpretability. Therefore, two system-level models of low- and mid-fidelity were created. The low-fidelity model was used to exemplify when the model is too simple for its purpose of assessing driving stability in crosswind conditions. The mid-fidelity model incorporated enough complexity to accurately emulate the response of the high-fidelity model, within certain tolerances. This setup provided knowledge about the necessary level of

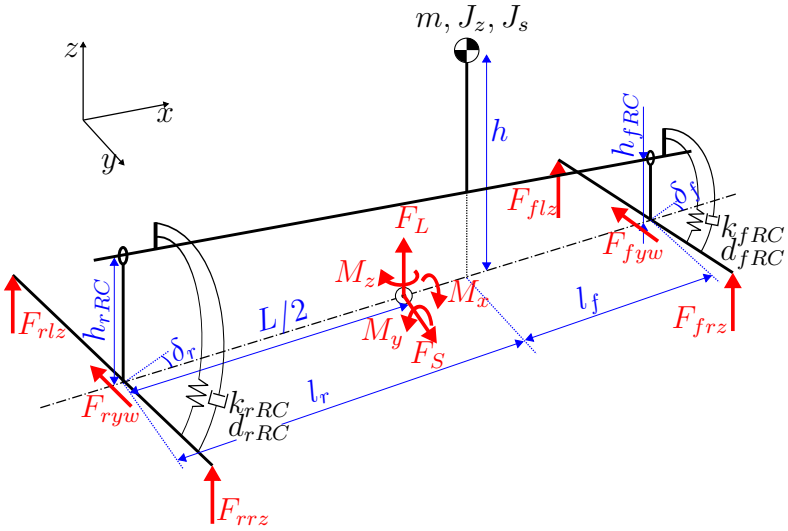

Figure 4.3: *The enhanced model (mid-fidelity), including the aerodynamic force play (F_S, F_L, M_x, M_y, M_z).*

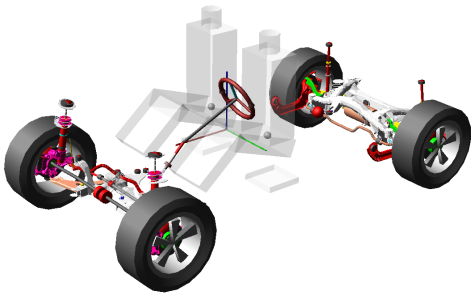

Figure 4.4: *The high fidelity model; a multi-body dynamic model built in Adams/Car software.*

model complexity for assessing straight-line driving stability. Moreover, the mid-fidelity model could be used to study the effects of the system properties in a parametric study.

4.2.1 Classical bicycle model (low fidelity)

The classical bicycle one-track model was used for comparison, as the low-fidelity model, in this study. The model has 2 degrees of freedom (DoF): lateral and yaw motion. The tires were modelled linearly with a lateral cornering stiffness coefficient, linearised around the static axle loads.

4.2.2 Enhanced model (mid fidelity)

The enhanced model was based on the bicycle model, but several additional vehicle properties were implemented to increase its accuracy for assessing driving stability at high speed. It was found that including a roll DoF improved the model (in line with the conclusions of a previous study on the effects of roll dynamic for crosswind sensitivity [19]). The lateral tire cornering stiffness was modelled, based on the normal load, using a 2^{nd} order polynomial. The polynomial was fitted to experimental tire data. Furthermore, the enhanced model accounted for kinematic and elasto-kinematic steering effects in the suspension system. Figure 4.3 shows a schematic view of the enhanced model.

4.2.3 Multi-body dynamic model (high fidelity)

A multi-body dynamic model was used as the reference model, with the highest fidelity. The model can be seen in Figure 4.4. It was built in Adams/Car, using the *PAC2002* [66] (Pacejka Magic Formula) tire model and had a Gruebler count of 2136 (approximate degrees of freedom).

4.2.4 Driver modelling

A simple driver model was used in all three vehicle dynamic models. The driver model used a locked steering angle, which was calculated to yield zero yaw velocity and lateral acceleration prior to the gust events.

4.2.5 Model validation

The motion response of the models was compared using the QSD approach based on tabulated windtunnel data as aerodynamic input, see Figure 4.5. The validation focused on the road plane motions: lateral acceleration and yaw velocity, since they correlated with the subjective stability performance in the experimental study. The high-fidelity model was used as reference. Evidently, the classical bicycle model (low fidelity) failed to emulate the response in terms of yaw velocity and lateral acceleration. Its response was slower with varying magnitude, acting as a too damped system. The enhanced model (mid fidelity) matched the response of the high-fidelity model well, proving that the essential system properties for this load case have been accurately implemented in this model.

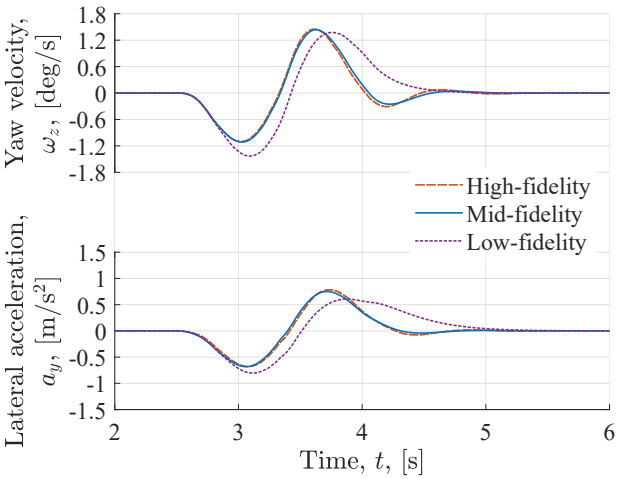

(a) *Profile 1.*

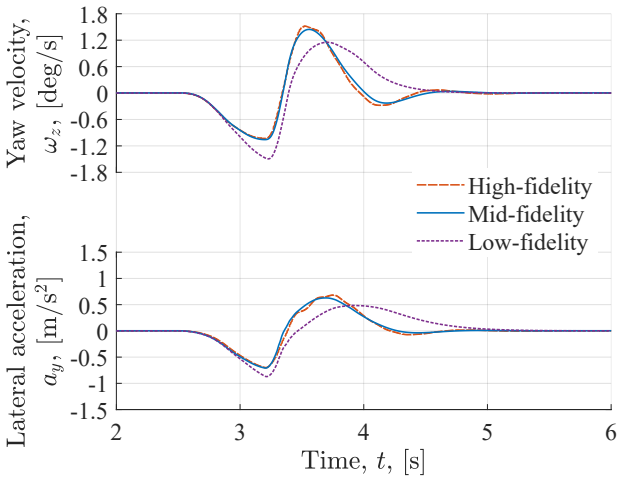

(b) *Profile 2.*

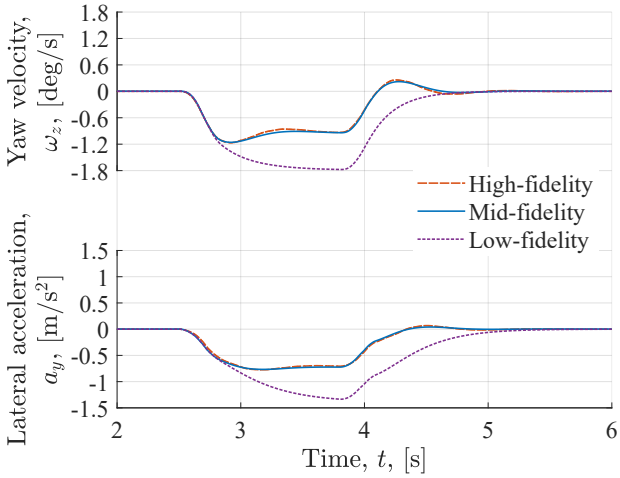

(c) *Profile 3.*

Figure 4.5: *Fidelity analysis; comparing the yaw velocity and lateral acceleration response during the gust profiles, for the three vehicle dynamics models.*

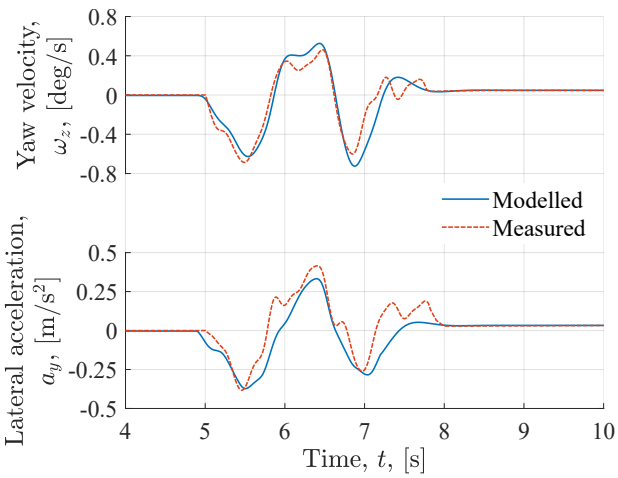

Figure 4.6: *Validation of the enhanced (mid-fidelity) model; comparing modelled versus measured yaw velocity and lateral acceleration response during crosswind gust event No. 8.*

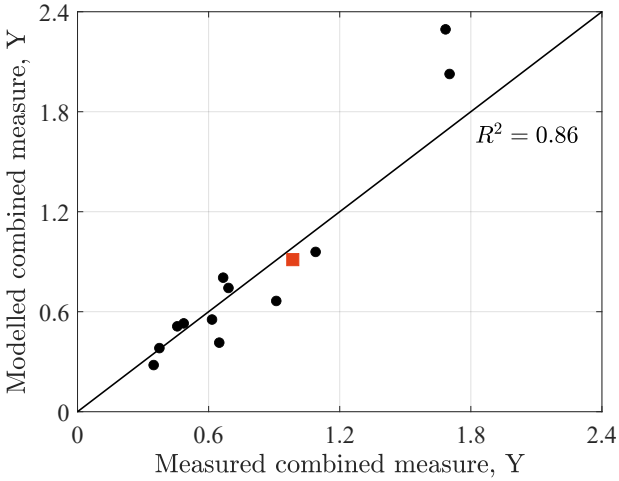

Figure 4.7: *Measured vs. modelled values of the combined measure, Y (Equation 3.2). The orange square corresponds to gust event No. 8, seen in Figure 4.6.*

To further justify the use of the enhanced model, a validation was performed using the experimental data set. Thirteen instances of experienced stability issues were selected from the data set. The measured vehicle motion response during the events could then be compared to the modelled response, where the vehicle-local wind measurements were converted to aerodynamic inputs using the quasi-steady approach. The driver steering input was also used as input to the enhanced model. Figure 4.6 shows the comparison for one of the instances. The model successfully captures the rapid changes and amplitude values in the measured data. All 13 instances were analysed, and Figure 4.7 compared the measured and modelled values of the combined measure (Equation 3.2). The diagonal line shows the ideal solution, where the modelled and measured values are equal. The data showed a fit of $R^2 = 0.86$ to the diagonal line, which was regarded acceptable considering the uncertainty of the measurement equipment and external disturbances (such as road unevenness) during the test track experiments. However, the model seemed to overpredict the response of the two strongest crosswind events. The highest driver steering wheel intervention was found at these events; hence, too simple modelling of the steering system could explain the overpredictions. Nevertheless, the studies presented in this work used a fixed steering wheel angle, and the simplified steering system did not affect those results. The orange square data point represents the instance seen in Figure 4.6.

4.3 Coupling methodology

The numerical coupling between aerodynamics and vehicle dynamics can principally be implemented in two ways. The most straightforward is to use a 1-way coupling, where the aerodynamic load is applied on the vehicle dynamic model, but the vehicle motion response does not affect the aerodynamics. The more authentic description would be to include the vehicle motion changes in the aerodynamic modelling, as in a 2-way coupling.

This work has performed a study on the necessity of a numerical 2-way coupling for SUV:s. The coupling was performed using the aerodynamic QSD model coupled to the enhanced (mid-fidelity) vehicle dynamic model. The QSD model uses the relative flow magnitude, V_{mag}, and angle, ψ, as inputs. By accounting for the vehicle body slip, β, the 2-way coupling could be implemented via the flow conditions, as in Figure 4.8. Note that the crosswind, w_y, was defined perpendicular to the motion vector of the vehicle, $v_v = \sqrt{v_x^2 + v_y^2}$. This, to focus on the physical coupling effects between aerodynamics and vehicle dynamics, while excluding the influence from a driver model. The longitudinal vehicle velocity, v_x, was kept constant. New

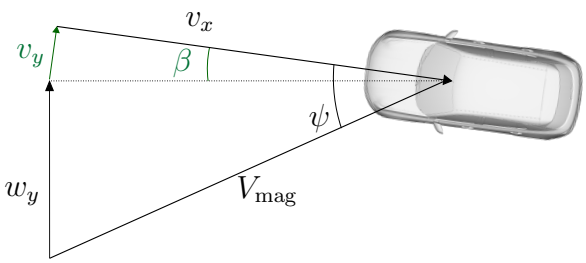

Figure 4.8: *Schematics of the implementation of the 2-way coupling between aerodynamics (QSD model) and vehicle dynamics (enhanced model) via the flow conditions. The relative flow magnitude, V_{mag}, and angle, ψ, accounts for the vehicle body slip angle, β.*

equations of the relative flow magnitude and angle could be derived from this formulation, see Equation 4.5 (to be compared with the 1-way coupling in Equation 2.6).

$$V_{\text{mag}} = \sqrt{v_x^2 + v_y^2 + w_y^2}, \qquad \psi = \arctan\left(\frac{w_y}{\sqrt{v_x^2 + v_y^2}}\right) + \beta. \tag{4.5}$$

4.4 Parametric analysis methodology

A numerical design of experiments was created to perform a parametric sensitivity study of vehicle dynamic and aerodynamic parameters. Time-efficient simulations of the crosswind response could be achieved by coupling the enhanced vehicle dynamic model to the aerodynamic QSD model. The proxy measure for stability (Equation 3.2) was used to evaluate the performance of each design.

Table 4.2: *Parameters and their intervals investigated in the sensitivity study.*

No.	Parameter	Abbr.	Unit	Max - Min
V1	Wheel base	whlB	m	0.40
V2	Track width	trkW	m	0.30
V3	Centre of gravity height	CoGz	m	0.40
V4	Centre of gravity position, l_f/L	CoGx	1	0.15
V5	Vehicle mass	mass	kg	1200
V6	Sprung mass moment of inertia (x)	inertx	kgm^2	350
V7	Mass moment of inertia (z)	inertz	kgm^2	2000
V8	Normalised tire lateral cornering stiffness	corStif	1/rad	10.0
V9	Side force steer, front	sStrFr	deg/kN	0.16
V10	Side force steer, rear	sStrRe	deg/kN	0.06
V11	Roll steer, front	rStrFr	deg/deg	0.11
V12	Roll steer, rear	rStrRe	deg/deg	0.07
V13	Roll centre height, front	rcFr	m	0.14
V14	Roll centre height, rear	rcRe	m	0.14
V15	Roll stiffness, front	rStifFr	Nm/deg	1800
V16	Roll stiffness, rear	rStifRe	Nm/deg	1500
A1	Side force coefficient gradient	side	1/deg	0.025
A2	Front lift coefficient at zero flow angle	fLift0	1	0.100
A3	Front lift coefficient quadratic increase	fLiftq	$1/\text{deg}^2$	0.001
A4	Rear lift coefficient at zero flow angle	rLift0	1	0.150
A5	Rear lift coefficient increase at 1.25 deg	rLift1	1	0.010
A6	Rear lift coefficient increase at 3.75 deg	rLift3	1	0.070
A7	Rear lift coefficient increase at 7.5 deg	rLift7	1	0.060
A8	Roll moment coefficient gradient	roll	1/deg	0.003
A9	Yaw moment coefficient gradient	yaw	1/deg	0.005

The sensitivity study included in total 25 vehicle parameters. Sixteen of those were vehicle dynamic parameter, having the prefix V in Table 4.2, and the nine aerodynamic parameters have the prefix A. The table shows the parameters' name, abbreviation, unit and investigated interval sizes between the minimum and maximum values. The nominal values were based on the existing vehicle and the intervals were selected from existing specifications and feasible spread in parameters for multiple vehicle types. Parameters V1-V7 capture the primary vehicle dynamic properties, such as wheel base (V1) and mass (V5). V8 is the input to the polynomial modelling the tire lateral cornering stiffness. Parameters V9-V16 are associated with suspension characteristics, a.k.a. kinematics and compliance (K&C) parameters. Side force steer (V9-V10) account for the additional steering of the suspension and steering system kinematics when side axle loads are applied, while the roll steer (V11-V12) does the same for the vehicle roll angle. The roll centre heights (V13-V14) and roll stuffiness (V15-V16) were also included as the final vehicle dynamic parameters.

The aerodynamic parameters were based on yaw sweep curves, where the aerodynamic coefficients of side force, roll moment and yaw moment often show a linear dependency on the flow angle. Hence, the A1, A8 and A9 parameters represent the linear gradient of the three quantities, respectively. The coefficient of front lift was modelled using two parameters, the first (A2) controlled the smallest value of front lift (at 0 deg flow angle), and the last (A3) controlled the quadratic increase of the coefficient at higher flow angles. Similarly, the coefficient of rear lift was controlled with four parameters, where the first (A4) controlled the smallest value of rear lift and the following (A5-A7) controlled the increase at higher flow angles. This modelling method of approximating the yaw sweep curves was only used in the parametric study to be able to evaluate their influence on crosswind stability. Otherwise, the exact yaw sweep curves were used in the quasi-steady approaches.

A Latin hypercube sampling was used as the design of experiments methodology. A total of 15 000 configurations were simulated, distributed between four parametric studies. The first study investigated the vehicle dynamic parameters, while keeping the aerodynamics constant at nominal values. The second study focused on the aerodynamics, while keeping the vehicle dynamic parameters constant. The third and largest study included all vehicle dynamic and aerodynamic parameters simultaneously. Finally, a study was performed with focus on the tire and suspension vehicle dynamic parameters (V8-V16). This was done since changing primary vehicle parameters (e.g., wheel base and centre of gravity position) most likely would be an unrealistic solution to improve crosswind stability.

The commercial optimisation software ModeFRONTIER 2017R5 was used to generate the Latin hypercube sampling, calculate the significant main effects (with a 95 % confidence level using t-distribution) and to create the response surfaces used to analyse the synergy effects. The response surfaces were based on radial basis functions.

4.5 Results and discussion

The results from the aerodynamic crosswind gust modelling will be presented first followed by the evaluation on coupling necessity and the results of the parametric sensitivity study.

4.5.1 Aerodynamic gust modelling

Figures 4.9a and 4.9b display the aerodynamic side force and yaw moment response, respectively. The figures present comparisons between the three crosswind gust profiles and between the three aerodynamic response modelling methods: quasi-steady (QS), quasi-steady with axle delay (QSD) and transient CFD (tCFD). The tCFD results were filtered through a 32 Hz low-pass filter, to improve visibility. As can be seen in Figure 4.9a, there is little difference in the side force response between the modelling methods (thin, thick and dashed lines). Both quasi-steady approaches neglect any transient fluid dynamic effects, and since the transient CFD (which account for those effects) showed similar results, it could be concluded that no significant transient effect of the side force is present during crosswind gusts of the magnitude and time interval investigated in this study. Furthermore, the modelling of the time delay between the axles had a small effect on the side force results (thick and dashed lines in Figure 4.9a).

The axle delay modelling had a more substantial effect on the yaw moment response (Figure 4.9b). Note especially the positive peak overshoot at 2.75 s of QSD profile 3 (black dashed) and the negative peak of QSD profile 2 (red dashed) at 3.4 s. These effects can be explained by the observation that in constant crosswind flow, the front axle side force work to turn the vehicle away from the crosswind (increasing the aerodynamic yaw moment), while the rear axle side force work in the opposite direction for the yaw moment, as demonstrated by Theissen [21]. The positive yaw moment overshoot at 2.75 s was hence a result of high front axle side force without any counteracting side force at the rear axle. The effect at 3.4 s is even more significant since the rapid change in flow angle resulted in a brief instance when the front and rear axle side force worked together to decrease the yaw moment to its negative peak value. This effect could be confirmed by the tCFD, which also showed a negative peak at 3.4 s and an overall better agreement with the QSD solution. Moreover, this also indicated that there was no significant transient fluid dynamic effect for the yaw moment either.

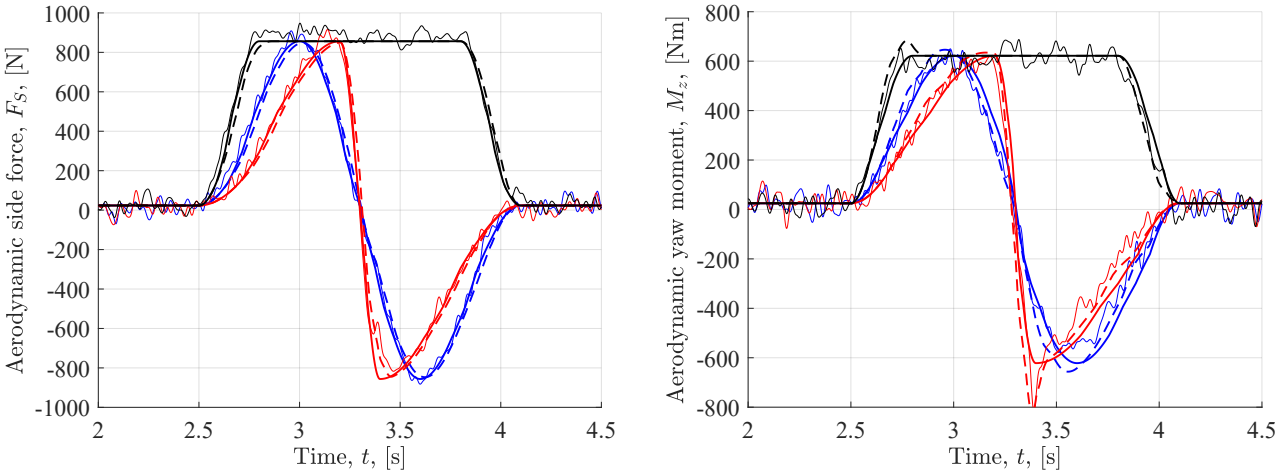

(a) *Side force.* **(b)** *Yaw moment.*

Figure 4.9: *The aerodynamic response for gust profile 1 (**blue**), profile 2 (**red**) and profile 3 (**black**), comparing tCFD (thin lines —) to QS (thick lines —) and QSD (thick dashed lines - - -) approaches.*

In summary, neither the aerodynamic side force, F_S, nor yaw moment, M_z, showed any transient fluid dynamic effects at these crosswind magnitudes and gust time intervals. Therefore, the QSD approach was regarded as an acceptable approximation of the aerodynamic response in this work. The overshoots of the aerodynamic yaw moment could be explained by the time delay between the front and rear axle when driving into crosswinds. Thus, increased aerodynamic admittance with increased gust frequency could be results of axle delay rather than a fluid dynamic hysteresis effect.

4.5.2 2-way coupling analysis

Figure 4.10 show the vehicle motion response comparing the 1-way and 2-way coupled solutions, for the three gust profiles. It is evident that the effects of the 2-way coupling (by accounting for the vehicle body slip) was negligible for an SUV at these crosswind conditions. Although the discrepancy between the coupling methods was slight, the largest effects were seen during gust profile 3 (Figure 4.10c).

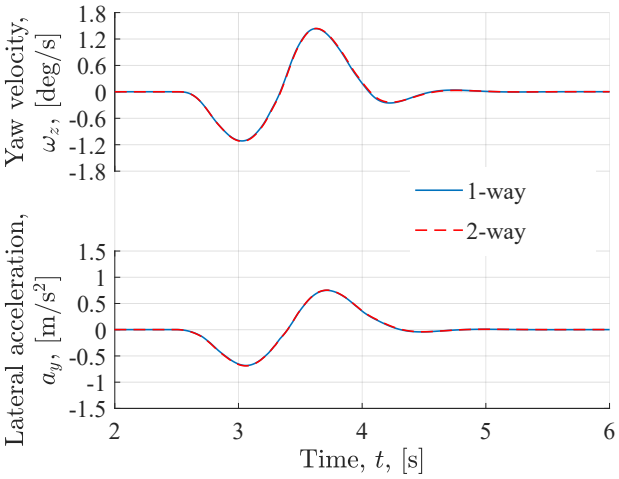

(a) *Profile 1.*

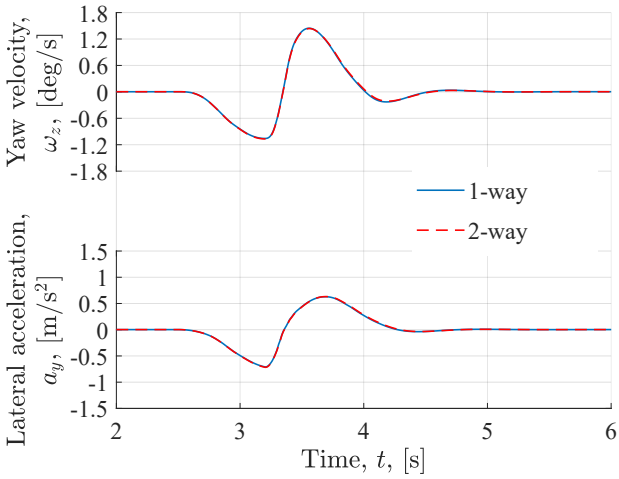

(b) *Profile 2.*

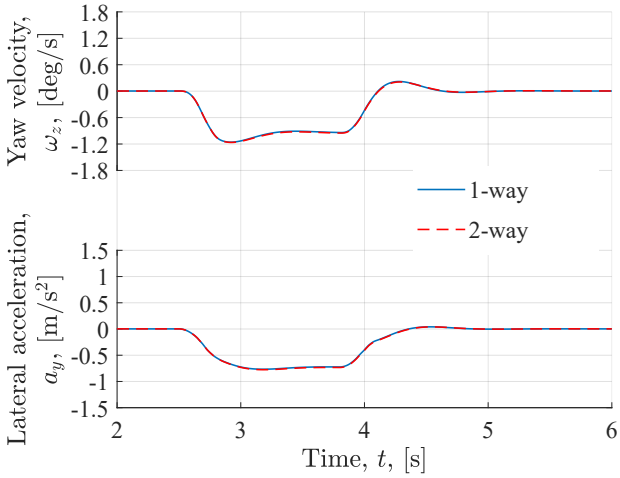

(c) *Profile 3.*

Figure 4.10: *The vehicle motion response in terms of yaw velocity, ω_z, and lateral acceleration, a_y, for the three gust profiles, comparing 1-way and 2-way coupled solutions.*

4.5.3 Parametric sensitivity analysis

The four parametric studies will follow.

Vehicle dynamic analysis

While keeping the aerodynamic parameters at constant nominal values, the 16 vehicle dynamic parameters were analysed. Figure 4.11 shows the main effects of the significant parameters, where only 8 of the 16 parameters proved to be significant for any of the aerodynamic load cases (gust profiles). The longitudinal centre of gravity position (V4) had the highest main effect, based on the chosen parameter intervals. The positive effect of 0.85 (profile 1) indicates that increasing V4, i.e. moving the centre of gravity (CoG) rearwards, would increase the vehicle motion response to the crosswind, and thus affect vehicle stability performance negatively. This effect was expected and have been seen in other studies [19, 36, 39, 40]. In general, it could be noted that the trend effect (sign) of each parameter was persistent regardless of gust profile, although the magnitude and level of significance varied. To minimise the yaw velocity response, increasing vehicle mass (V5) and yaw moment of inertia (V7) proved to be beneficial. Figure 4.11 also demonstrates the importance of wheel base (V1), tire lateral cornering stiffness (V8) and finally, the rear and front axle side force steer gradients (V10 and V9) and the rear axle roll stiffness (V16). Even though V9, V10 and V16 had small main effects, it was regarded as an interesting finding since it showed that suspension characteristics have potential to influence stability when primary vehicle parameters cannot be altered.

Aerodynamic analysis

The second analysis focused on the nine aerodynamic parameters, while keeping the vehicle dynamic parameters at nominal values. The significant main effects can be seen in Figure 4.12. It is evident that the aerodynamic yaw moment coefficient gradient (A9) had an effect size comparable to the vehicle dynamic effect V4, while the gradients of the side force (A1) and the roll moment (A8) coefficients had very small effects. The driving stability in crosswinds can thus be improved by reducing the gradient of the yaw moment coefficient (C_{ym}), i.e. moving centre of pressure (CP) rearwards (Figure 2.4).

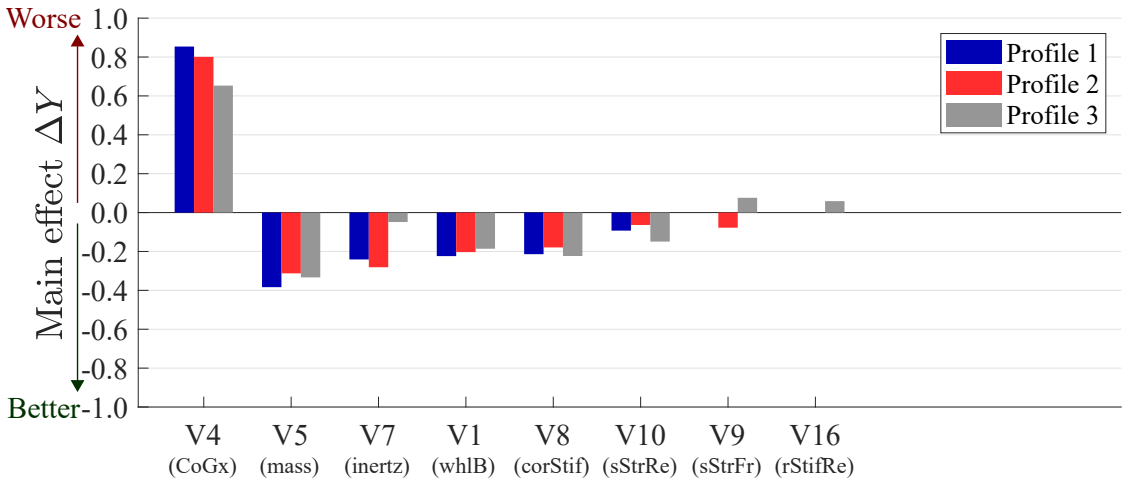

Figure 4.11: *The main effects of the significant vehicle dynamic parameters. Positive values indicate higher (worse) vehicle motion response when increasing the parameter.*

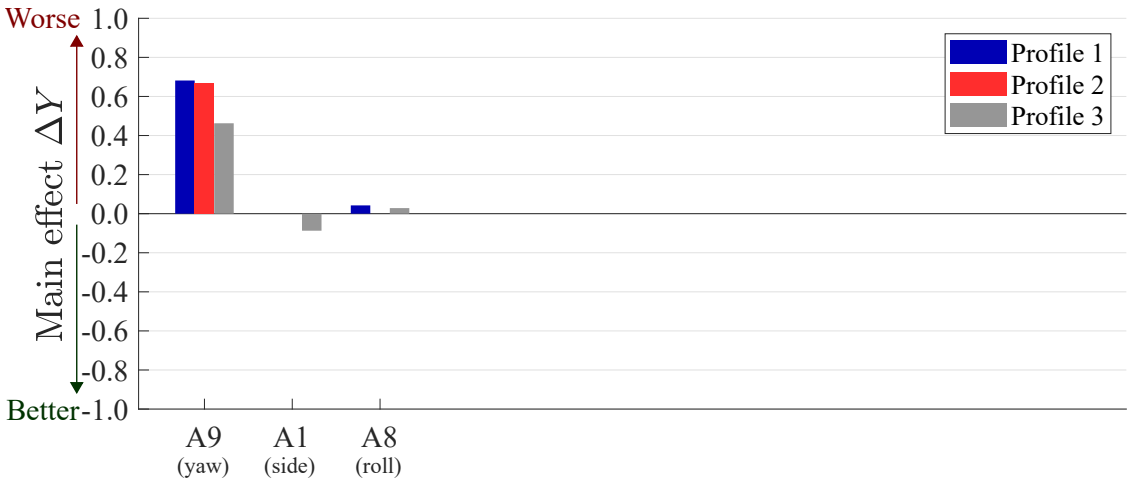

Figure 4.12: *The main effects of the significant aerodynamic parameters.*

Combined analysis

Figure 4.13 show the significant main effects out of all 25 parameters. Most significant parameters from the vehicle dynamic analysis were also found significant in the combined analysis, along with the aerodynamic yaw moment coefficient (A9), side force coefficient (A1) and rear axle lift coefficient (A4) The effects were similar in size in the combined analysis, as in the separate analyses, indicating low synergy between the most important parameters. The combined analysis also showed new significant parameters for profile 3, namely the CoG height (V3) and rear axle lift force (A4). Nevertheless, these parameters had small effects and the general recommendations for decreasing crosswind sensitivity are to move CoG forwards and reduce the aerodynamic yaw moment coefficient, if possible. Furthermore, it should be noted that increasing the vehicle mass (V5), which is negative for many vehicle attributes, would improve the straight-line driving stability performance during crosswinds.

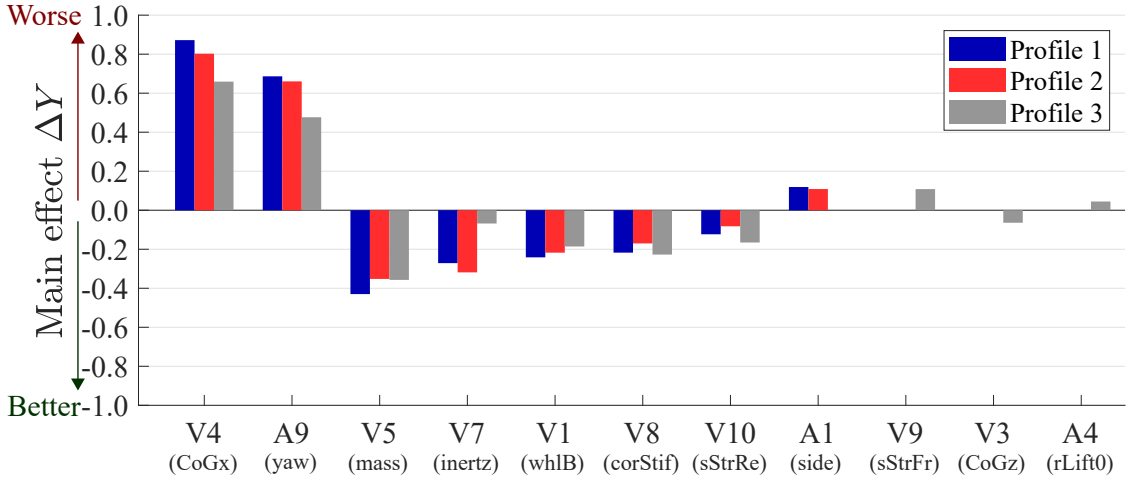

Figure 4.13: *The main effects of the significant vehicle dynamic and aerodynamic parameters combined.*

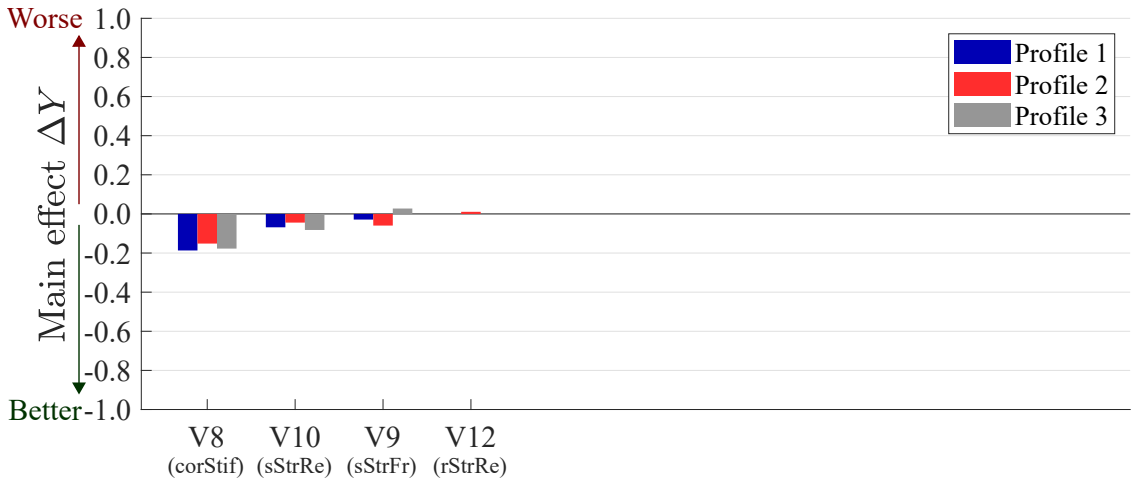

Figure 4.14: *The main effects of the significant realistic vehicle dynamic parameters.*

Tire and wheel suspension analysis

Since many attributes need to be taken into consideration when designing a passenger vehicle, it might not be an alternative to alter the position of CoG, mass, wheel base or other primary vehicle parameters. Therefore, a fourth parametric analysis was conducted only focusing on suspension and tire parameters (V8-V16), while keeping the other vehicle dynamic and aerodynamic parameters at constant nominal values. Four out of the seven parameters proved to have significant main effects, see Figure 4.14. The tire lateral cornering stiffness (V8) had the highest main effect where stiffer tires seemed to improve driving stability by lowering the vehicle response to crosswinds. The side force steer gradients (V9 and V10) had significant main effects, but also an interesting synergy between axles see Figure 4.15. The minimum seen in the figure represents when the side force steering increases the axle understeering at the rear and decreases it at the front. In summary, these results prove that it is possible to improve crosswind driving stability at high speeds without altering the primary vehicle dynamic parameters.

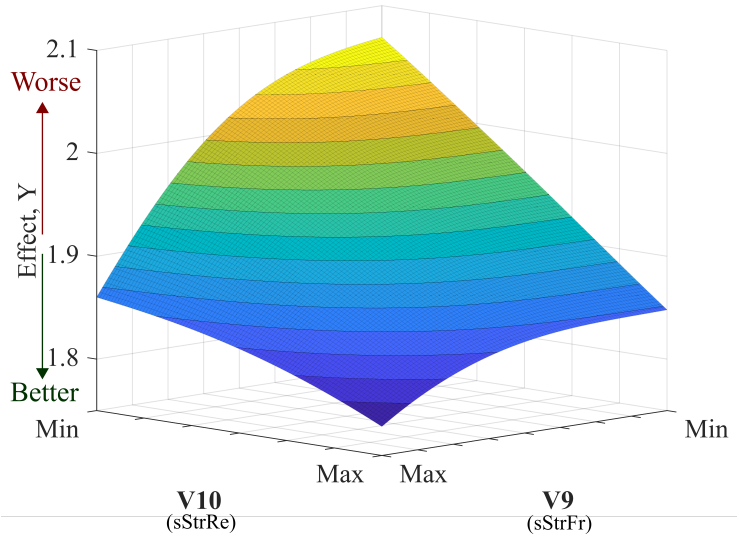

Figure 4.15: *Visualisation of the synergy effect between parameters V9 and V10.*

5

Concluding remarks

The purpose of this thesis has been twofold. First, to understand the dynamics of the coupled aerodynamic/vehicle dynamic system during high speed driving in crosswind conditions, but also to find virtual objective tools for assessing the driving stability performance of passenger vehicles. This has been done both experimentally, during the on-track measurements, and numerically using the crosswind simulation methodology developed in this thesis.

The experimental study at the high speed test track focused on correlating the drivers' subjective assessment of stability issues with certain wind loads and with certain motions of the vehicle body. To conduct this correlation, the test vehicle was instrumented with a wind probe on the roof, equipment for measuring the vehicle motion response and a subjective trigger button in the cabin. The subjective trigger could be pressed by the drivers when stability issues were experienced, which would generate a time stamp in the measured data. This setup enabled the objective correlation between higher changes in crosswind and worse stability performance, where the performance was affected already at crosswind changes of 5 m/s and above. Furthermore, higher variations in lateral acceleration and yaw velocity of the vehicle body did also correlate with increased frequency of trigger events of stability issues. Hence, it could be concluded that these road-plane vehicle motions were, at least partly, the cause of the subjective perception of poorer driving stability. These results were used to formulate an objective proxy measure for driving stability, to be used in virtual assessments.

The objective measure could be used to evaluate the driving stability performance of vehicle configurations in the numerical study. The numerical study aimed at developing a coupled simulation methodology for driving stability under crosswinds and to gain insights on key vehicle parameters affecting the dynamics of the system. Three crosswinds gust profiles (based on the findings of the on-track measurements) were applied in the modelling of the aerodynamic forces. A transient crosswind simulation strategy was compared with two quasi-steady approaches of approximating the aerodynamic load, where one of them accounted for the phase delay of the flow between the front and rear axle when driving into crosswind conditions. The results showed that that the quasi-steady approach with axle delay (QSD) could mimic the response seen when simulating the full transient gust event. Even the overshoots in the yaw moment seen when rapidly changing flow angle were accurately modelled. Hence, it could be concluded that the QSD approach could be used to approximate the aerodynamic load at the gust amplitudes of ± 5 m/s with the frequency corresponding to 16 vehicle lengths. The aerodynamic loads were coupled with vehicle dynamic models, to estimate the vehicle motion responses to the gusts and to determine the driving stability performance using the objective measure. Three

vehicle dynamic models of varying fidelity (low, mid and high) were investigated. One of them (mid-fidelity) was developed in the numerical study, with the intent of showing the level of complexity needed to emulate the same response as the high-fidelity reference model. This was achieved by adding roll dynamics, non-linear tire cornering stiffness and certain suspension characteristics to the bicycle model. The mid-fidelity (enhanced) model was further validated with the experimental on-track data, where the model accurately predicted the measured vehicle motion response based on the measured wind and driver steering response. The classical bicycle model (low-fidelity) was included to exemplify a lack of complexity for approximating the vehicle response to crosswinds. The numerical study did also analyse the effect and necessity of a 2-way coupled simulation methodology, between aerodynamics and vehicle dynamics. It was concluded that the 2-way coupling had negligible effects compared to the 1-way coupling, for an SUV in these crosswinds conditions. An extensive parametric study was performed using the 1-way coupled QSD/enhanced model simulation methodology. It was shown that the longitudinal position of the centre of gravity had the highest influence on crosswind stability. By moving the centre of gravity forward, the driving stability could be improved. The aerodynamic parameter with the highest influence was the gradient of the yaw moment coefficient. As expected, reducing the gradient and thus moving the centre of pressure rearwards improved stability. Other significant parameters were, e.g., the vehicle mass and wheel base where higher values were found beneficial. However, these primary parameters affect many other vehicle attributes and may not be realistic solutions for improving the driving stability performance. Fortunately, the parametric study could also conclude that certain tire and suspension characteristics could improve the stability performance at high speeds. The balance of the side force steer gradient between the front and rear axle along with the tire cornering stiffness had a significant effect on the vehicle response, although the effects were much smaller than those of the centre of gravity and aerodynamic yaw moment.

5.1 Future work

So far, a general understanding has been formed about the interdisciplinary physics and how to assess driving stability virtually using coupled simulation methodologies. This is essential for the continued work of setting better engineering requirements and further improve the virtual tools.

Future work is planned to utilise a state of the art motion platform driving simulator to verify that high changes in lateral acceleration and yaw velocity are perceived as issues with driving stability. The simulator may also be used as an intermediate tool for assessing stability, between the on-track testing and the numerical simulations. The progress of autonomous vehicles initiates additional interesting topics on driving stability and what the new customer requirements are for trusting an autonomous system. It is generally believed that this will increase the demands for high driving stability performance.

The present numerical investigation on aerodynamics included crosswinds of a single time scale (and length scale). It would be of interest to extend the virtual tools by assessing the aerodynamic admittance at a frequency spectrum and combining the response of the complete system. This will require development of a suitable human-like driver model to be included in the system. Furthermore, autonomous driver models can be interchange with the human

models to evaluate differences and improve the autonomous algorithms. Automatic/autonomous steering can also lead to an additional set of design parameters (control algorithms and their parameters), compared to the traditional (mechanical and geometric) vehicle dynamics and aerodynamics design parameters.

6

Summary of papers

6.1 Paper A

Quantitative High Speed Stability Assessment of a Sports Utility Vehicle and Classification of Wind Gust Profiles

This paper is focused on finding realistic aerodynamic load cases for driving stability at high speed. In addition, the study aimed at correlating the drivers' subjective assessment of poorer stability performance to quantitative objective measures of the vehicle body motion. The experimental work was performed at the high speed track at Hällered Proving Ground using a compact SUV. The vehicle was instrumented with a wind probe, equipment for measuring the vehicle motion and trigger button for the drivers' to note issues with the driving stability performance. The correlation between the subjective perception of stability issues and the change in lateral acceleration and yaw velocity is shown in the paper. Also, it is shown that crosswinds seldom generate flow angles above 10 deg at high speed driving. Nevertheless, already weaker crosswinds of ± 5 m/s (± 6.4 deg at 160 km/h) deteriorated the driving stability, indicating the importance of studying crosswinds stability. The paper mathematically defines a set of typical crosswind gusts.

6.2 Paper B

High Speed Driving Stability of Road Vehicles under Crosswinds: An aerodynamic and vehicle dynamic parametric sensitivity analysis

This paper uses the findings of Paper A to develop a virtual assessment of driving stability using coupled simulation tools. The crosswind gust profiles are used in the aerodynamic modelling and the correlated vehicle motions are used in a proxy measure for driving stability. By comparing three methods of modelling the aerodynamic response, it is shown that the flow delay between the axles when driving into crosswinds is important. The paper presents a quasi-steady model which accounts for this. Furthermore, the level of complexity needed to assess crosswinds stability in the vehicle dynamic models is investigated. Finally, the paper includes a parametric study of the coupled simulation model. The study primarily highlights the importance of the longitudinal centre of gravity position and the gradient of the aerodynamic yaw moment coefficient. Nevertheless, other parameters are also found significant including some tire and suspension characteristics.

References

[1] Brandt, A. et al. "Quantitative High Speed Stability Assessment of a Sports Utility Vehicle and Classification of Wind Gust Profiles". *SAE Technical Paper Series*. 2020. DOI: 10.4271/2020-01-0677.

[2] Brandt, A., Jacobson, B., and Sebben, S. "High Speed Driving Stability of Road Vehicles under Crosswinds: An aerodynamic and vehicle dynamic parametric sensitivity analysis". *Submitted to Vehicle System Dynamics* (2020).

[3] Baker, C. J. and Reynolds, S. "Wind-induced accidents of road vehicles". *Accident Analysis & Prevention* **24**.6 (1992), 559–575. DOI: 10.1016/0001-4575(92)90009-8.

[4] Sims-Williams, D. "Cross Winds and Transients: Reality, Simulation and Effects". *SAE International Journal of Passenger Cars - Mechanical Systems* **4**.1 (2011), 172–183. DOI: 10.4271/2011-01-0172.

[5] Howell, J. et al. "The Effect of a Sheared Crosswind Flow on Car Aerodynamics". *SAE Int. J. Passeng. Cars - Mech. Syst.* **10**.1 (2017), 278–285. DOI: https://doi.org/10.4271/2017-01-1536.

[6] Wordley, S. and Saunders, J. W. "On-road Turbulence". *SAE Int. J. Passeng. Cars – Mech. Syst.* **1**.1 (2008), 341–360. DOI: https://doi.org/10.4271/2008-01-0475.

[7] Wordley, S. and Saunders, J. W. "On-road Turbulence: Part 2". *SAE International Journal of Passenger Cars - Mechanical Systems* **2**.1 (2009), 111–137. DOI: 10.4271/2009-01-0002.

[8] Watkins, S. and Cooper, K. R. "The Unsteady Wind Environment of Road Vehicles, Part Two: Effects on Vehicle Development and Simulation of Turbulence". *SAE Technical Paper Series*. 2007. DOI: 10.4271/2007-01-1237.

[9] Cooper, K. R. and Watkins, S. "The Unsteady Wind Environment of Road Vehicles, Part One: A Review of the On-road Turbulent Wind Environment". *SAE Technical Paper Series*. 2007. DOI: 10.4271/2007-01-1236.

[10] MacAdam, C. C. et al. "Crosswind Sensitivity of Passenger Cars and the Influence of Chassis and Aerodynamic Properties on Driver Preferences". *Vehicle System Dynamics* **19**.4 (1990), 201–236. DOI: 10.1080/00423119008968942.

[11] Fukagawa, T. et al. "Modeling of Transient Aerodynamic Forces based on Crosswind Test". *SAE Int. J. Passeng. Cars - Mech. Syst.* **9**.2 (2016), 572–582. DOI: https://doi.org/10.4271/2016-01-1577.

[12] Nakasato, K. et al. "Coupled 6DoF Motion and Aerodynamic Crosswind Simulation Incorporating Driver Model". *SAE Int. J. Passeng. Cars - Mech. Syst.* **10**.2 (2017), 662–670. DOI: https://doi.org/10.4271/2017-01-1525.

[13] Lewington, N. et al. "The Application of a One-Way Coupled Aerodynamic and Multi-Body Dynamics Simulation Process to Predict Vehicle Response during a Severe Crosswind Event". *SAE Technical Paper Series*. SAE International, 2017. DOI: https://doi.org/10.4271/2017-01-1515.

[14] "Road vehicles – Sensitivity to lateral wind – Open-loop test method using wind generator input". ISO 12021:2010.

[15] Forbes, D. C. et al. "A Fully Coupled, 6 Degree-of-Freedom, Aerodynamic and Vehicle Handling Crosswind Simulation using the DrivAer Model". *SAE International Journal of Passenger Cars - Mechanical Systems* **9**.2 (2016). DOI: 10.4271/2016-01-1601.

[16] Carbonne, L., Winkler, N., and Efraimsson, G. "Use of Full Coupling of Aerodynamics and Vehicle Dynamics for Numerical Simulation of the Crosswind Stability of Ground Vehicles". *SAE International Journal of Commercial Vehicles* **9**.2 (2016), 359–370. DOI: 10.4271/2016-01-8148.

[17] Li, S. Y. et al. "Coupled analysis of vehicle stability in crosswind on low adhesion road". *International Journal of Numerical Methods for Heat & Fluid Flow* **28**.8 (2018), 1956–1972. DOI: 10.1108/hff-01-2018-0013.

[18] Huang, T. et al. "Investigation of vehicle stability under crosswind conditions based on coupling methods". *Proceedings of the Institution of Mechanical Engineers, Part D: Journal of Automobile Engineering* (2019). DOI: 10.1177/0954407018822424.

[19] Tunay, T., O'Reilly, C. J., and Drugge, L. "The Significance of Roll on the Dynamics of Ground Vehicles Subjected to Crosswind Gusts by Two-Way Coupled Simulation of Aero- and Vehicle Dynamics". *Advances in Dynamics of Vehicles on Roads and Tracks*. Lecture Notes in Mechanical Engineering. 2020, pp. 1388–1397. DOI: 10.1007/978-3-030-38077-9_160.

[20] Wojciak, J. "Quantitative Analysis of Vehicle Aerodynamics during Crosswind Gusts". PhD thesis. Technical University of Munich, 2012.

[21] Theissen, P. "Unsteady Vehicle Aerodynamics in Gusty Crosswind". PhD thesis. Technical University of Munich, 2012.

[22] Jessing, C. et al. "Investigation of Transient Aerodynamic Effects on Public Roads in Comparison to Individual Driving Situations on a Test Site". *SAE Technical Paper Series*. 2020. DOI: 10.4271/2020-01-0670.

[23] Onishi, Y. et al. "On Road Fuel Economy Impact by the Aerodynamic Specifications under the Natural Wind". *SAE Technical Paper Series*. 2020. DOI: 10.4271/2020-01-0678.

[24] Lawson, A. A., Sims-Williams, D. B., and Dominy, R. G. "Effects of On-Road Turbulence on Vehicle Surface Pressures in the A-Pillar Region". *SAE International Journal of Passenger Cars - Mechanical Systems* **1**.1 (2008), 333–340. DOI: 10.4271/2008-01-0474.

[25] Wagner, A. and Wiedemann, J. "Crosswind Behavior in the Driver 's Perspective". *SAE Technical Paper Series* 724 (2002). DOI: 10.4271/2002-01-0086.

[26] Song, J. et al. "Characteristics of Flow Behind a Passenger Vehicle". *SAE Technical Paper Series*. 2006. DOI: 10.4271/2006-01-1030.

[27] Krantz, W. "An Advanced Approach for Predicting and Assessing the Driver's Response to Natural Crosswind". PhD thesis. University of Stuttgart, 2012.

[28] Kumar, A. et al. "Analysis of Subjective Qualitative Judgement of Passenger Vehicle High Speed Drivability due to Aerodynamics". *Energies* **12**.14 (2019). DOI: 10.3390/en12142839.

[29] Willumeit, H. P. et al. "Method to Correlate Vehicular Behaviour and Driver's Judgement under Side Wind Disturbances". *Vehicle System Dynamics* **17** (1988), 508–524. DOI: 10.1080/00423118808969292.

[30] "Road vehicles – Vehicle dynamics and road-holding ability – Vocabulary". ISO 8855:2011.

[31] Hucho, W.-H. "Aerodynamics of Road Vehicles". Fourth edition. SAE International, 1998.

[32] Barth, R. “Effect of Unsymmetrical Wind Incidence on Aerodynamic Forces Acting on Vehicle Models and Similar Bodies”. SAE International, 1965. DOI: https://doi.org/10.4271/650136.

[33] Favre, T. et al. “Static coupling between detached-eddy simulations and vehicle dynamic simulations of a generic road vehicle model with different rear configurations in unsteady crosswind”. *International Journal of Vehicle Design* **72**.4 (2016). DOI: 10.1504/ijvd.2016.082384.

[34] “Vehicle Aerodynamics Terminology”. SAE J1594 JUL2010.

[35] Milliken, W. F., Dell’Amico, F., and Rice, R. S. “The Static Directional Stability and Control of the Automobile”. *SAE Technical Paper Series*. 1976. DOI: 10.4271/760712.

[36] Buchheim, R., Maretzke, J., and Piatek, R. “The Control of Aerodynamic Parameters Influencing Vehicle Dynamics”. *SAE Paper* (1985), 850279–850279. DOI: 10.4271/850279.

[37] Howell, J. and Le Good, G. “The Influence of Aerodynamic Lift on High Speed Stability”. *SAE Technical Paper SeriesTechnial* **01**.0651 (1999), 8–8. DOI: 10.4271/1999-01-0651.

[38] Windsor, S. and Le Good, G. “The Influence of Aerodynamic Lift on High Speed Stability”. *Autotech 93*. Vol. 01. 1993, pp. 8–8.

[39] Oraby, W. A. H. and Crolla, D. A. “Passenger Car Stability Under Random Wind Excitation”. *SAE Technical Paper Series*. SAE International, 2001. DOI: https://doi.org/10.4271/2001-01-0133.

[40] Juhlin, M. and Eriksson, P. “A Vehicle Parameter Study on Crosswind Sensitivity of Buses”. *SAE Technical Paper Series*. 2004. DOI: 10.4271/2004-01-2612.

[41] Howell, J. and Panigrahi, S. “Aerodynamic Side Forces on Passenger Cars at Yaw”. *SAE Technical Paper Series*. 2016. DOI: 10.4271/2016-01-1620.

[42] Chadwick, A., Garry, K., and Howell, J. “Transient Aerodynamic Characteristics of Simple Vehicle Shapes by the Measurement of Surface Pressures”. *SAE Technical Paper Series* (2000). DOI: https://doi.org/10.4271/2000-01-0876.

[43] Davenport, A. G. “THE APPLICATION OF STATISTICAL CONCEPTS TO THE WIND LOADING OF STRUCTURES”. *Proceedings of the Institution of Civil Engineers* (1961).

[44] Schroeck, D. et al. “Unsteady Aerodynamic Properties of a Vehicle Model and their Effect on Driver and Vehicle under Side Wind Conditions”. *SAE Int. J. Passeng. Cars – Mech. Syst.* **4**.1 (2011), 108–119. DOI: https://doi.org/10.4271/2011-01-0154.

[45] Stoll, D. and Wiedemann, J. “Active Crosswind Generation and Its Effect on the Unsteady Aerodynamic Vehicle Properties Determined in an Open Jet Wind Tunnel”. SAE International, 2018. DOI: https://doi.org/10.4271/2018-01-0722.

[46] Fuller, J. B. and Passmore, M. “Unsteady Aerodynamics of an Oscillating Fastback Model”. *SAE International Journal of Passenger Cars - Mechanical Systems* **6**.1 (2013), 403–413.

[47] Oettle, N. et al. “Assessment of a Vehicle’s Transient Aerodynamic Response”. *SAE Technical Paper Series*. 2012. DOI: 10.4271/2012-01-0449.

[48] Kawakami, M., Murata, O., and Maeda, K. “Improvement in Vehicle Motion Performance by Suppression of Aerodynamic Load Fluctuations”. *SAE International Journal of Passenger Cars - Mechanical Systems* **8**.1 (2015), 205–216. DOI: 10.4271/2015-01-1537.

[49] Jarlmark, J. "Driver-vehicle interaction under influence of crosswind gust". Licentiate thesis. Royal Institute of Technology, 2002.

[50] Klasson, J. "A Generalised Crosswind Model for Vehicle Simulation Purposes". *Vehicle System Dynamics* **3114** (2001). DOI: 10.1080/00423114.2002.11666245.

[51] Juhlin, M. "Aerodynamic loads on buses due to crosswind gusts – on-road measurements". *Vehicle System Dynamics* **46**.sup1 (2008), 827–835. DOI: 10.1080/00423110802037081.

[52] Drugge, L. and Juhlin, M. "Aerodynamic loads on buses due to crosswind gusts: extended analysis". *Vehicle System Dynamics* **48**.sup1 (2010), 287–297. DOI: 10.1080/00423111003739814.

[53] Mankowski, O., Sims-Williams, D., and Dominy, R. "A Wind Tunnel Simulation Facility for On-Road Transients". *SAE International Journal of Passenger Cars - Mechanical Systems* **7**.3 (2014), 1087–1095. DOI: 10.4271/2014-01-0587.

[54] Favre, T. "Aerodynamics simulations of ground vehicles in unsteady crosswind". PhD thesis. Royal University of Technology, 2011.

[55] Winkler, N. et al. "Coupling aerodynamics to vehicle dynamics in transient crosswinds including a driver model". *Computers & Fluids* **138** (2016), 26–34. DOI: 10.1016/j.compfluid.2016.08.006.

[56] Nakashima, T. et al. "Coupled analysis of unsteady aerodynamics and vehicle motion of a road vehicle in windy conditions". *Computers & Fluids* **80** (2013), 1–9. DOI: 10.1016/j.compfluid.2012.09.028.

[57] Huang, T. et al. "Transient aerodynamics simulations of a road vehicle in the crosswind condition coupled with the vehicle's motion". *Proceedings of the Institution of Mechanical Engineers, Part D: Journal of Automobile Engineering* **232**.5 (2017), 583–598. DOI: 10.1177/0954407017704609.

[58] Nakashima, T. et al. "HPC-LES for Unsteady Aerodynamics of a Heavy Duty Truck in Wind Gust - 2nd report: Coupled Analysis with Vehicle Motion". *SAE Technical Paper Series*. 2010. DOI: 10.4271/2010-01-1021.

[59] Aeroprobe Corporation. "Standard Probe User Manual, Document No. 90001-02-UMN-02". Catalog. 2015.

[60] Schuetz, T. "Aerodynamics of Road Vehicles". Fifth Edition. 2015. ISBN: 978-0-7680-7977-7. DOI: 10.4271/r-430.

[61] Dewesoft GmbH. "DS-IMU/Gyro User Manual". Catalog. 2013.

[62] "Hällered Test track, Sweden - Aerial Shot". Web Page. Accessed: 2020-12-15. URL: https://www.media.volvocars.com/global/en-gb/media/photos/35609.

[63] Favre, T. and Efraimsson, G. "An Assessment of Detached-Eddy Simulations of Unsteady Crosswind Aerodynamics of Road Vehicles". *Flow, Turbulence and Combustion* **87**.1 (2011), 133–163. DOI: 10.1007/s10494-011-9333-4.

[64] Menter, F. "Stress-Blended Eddy Simulation (SBES)—A New Paradigm in Hybrid RANS-LES Modeling". *Progress in Hybrid RANS-LES Modelling*. Notes on Numerical Fluid Mechanics and Multidisciplinary Design. Springer International Publishing, 2018. Chap. Chapter 3, pp. 27–37. ISBN: 978-3-319-70030-4 978-3-319-70031-1. DOI: 10.1007/978-3-319-70031-1_3.

[65] Ekman, P. et al. "Accuracy and Speed for Scale-Resolving Simulations of the DrivAer Reference Model". *SAE Technical Paper Series*. 2019. DOI: 10.4271/2019-01-0639.

[66] Kuiper, E. and Van Oosten, J. J. M. "The PAC2002 advanced handling tire model". *Vehicle System Dynamics* **45** (2007), 153–167. DOI: 10.1080/00423110701773893.